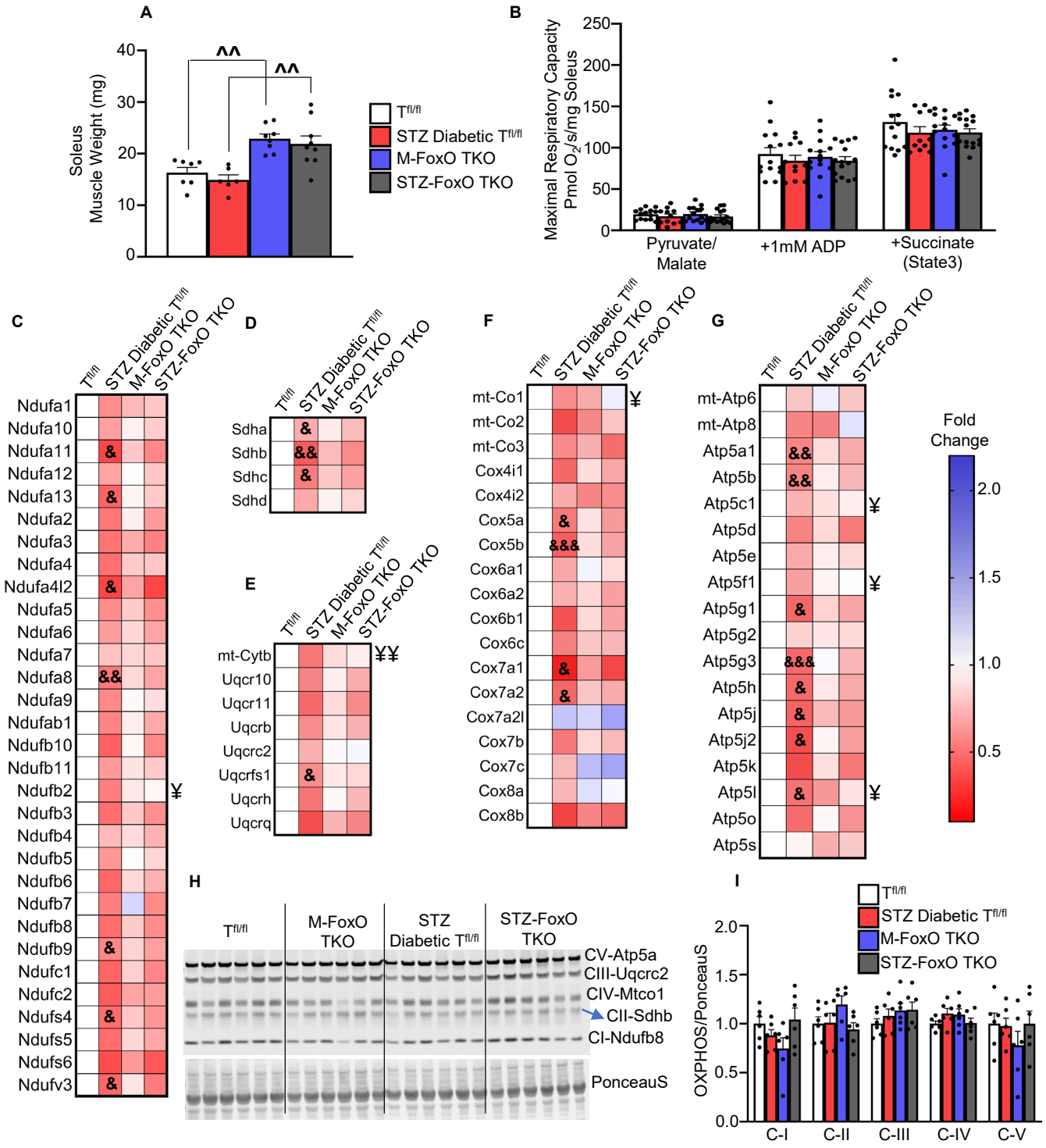

Supplemental Figure 1. Soleus fiber respiration and OXPHOS proteins were unchanged in STZ diabetic $T^{fl/fl}$ and STZ-FoxO TKO muscle, whereas decreased OXPHOS genes in STZ diabetic $T^{fl/fl}$ are normalized following deletion of FoxOs in STZ-FoxO TKO muscle. (A) Muscle weight of soleus from $T^{fl/fl}$ controls, STZ diabetic $T^{fl/fl}$, M-FoxO TKO, and STZ-FoxO TKO (n=6-9). **(B)** Maximal respiratory capacity in soleus fibers from STZ diabetic $T^{fl/fl}$ and STZ FoxO-TKO muscle and non-diabetic controls (n=11-15). **(C-G)** Heat map displaying RNA-Seq transcript levels of OXPHOS subunits of complex I, excluding core complex subunits (C). Transcript levels of subunits from complexes II (D), CIII (E), CIV (F), and CV (G) in quad from controls, STZ diabetic $T^{fl/fl}$, M-FoxO TKO, and STZ-FoxO TKO (n=4-6). **(H** and **I)** Western blot image (H) and densitometry (I) of OXPHOS proteins in quad from STZ diabetic $T^{fl/fl}$ and STZ-FoxO TKO muscle (n=6). Results represented as the mean ± SEM. (^^ p<0.01 as indicated Two-way ANOVA; &-FDR<0.05, &&-FDR<0.01 STZ diabetic $T^{fl/fl}$ vs. Control $T^{fl/fl}$; ¥-p<0.05, ¥¥-p<0.01 ratio of STZ-FoxO TKO/M-FoxO TKO versus STZ diabetic $T^{fl/fl}$/citrate-treated $T^{fl/fl}$).

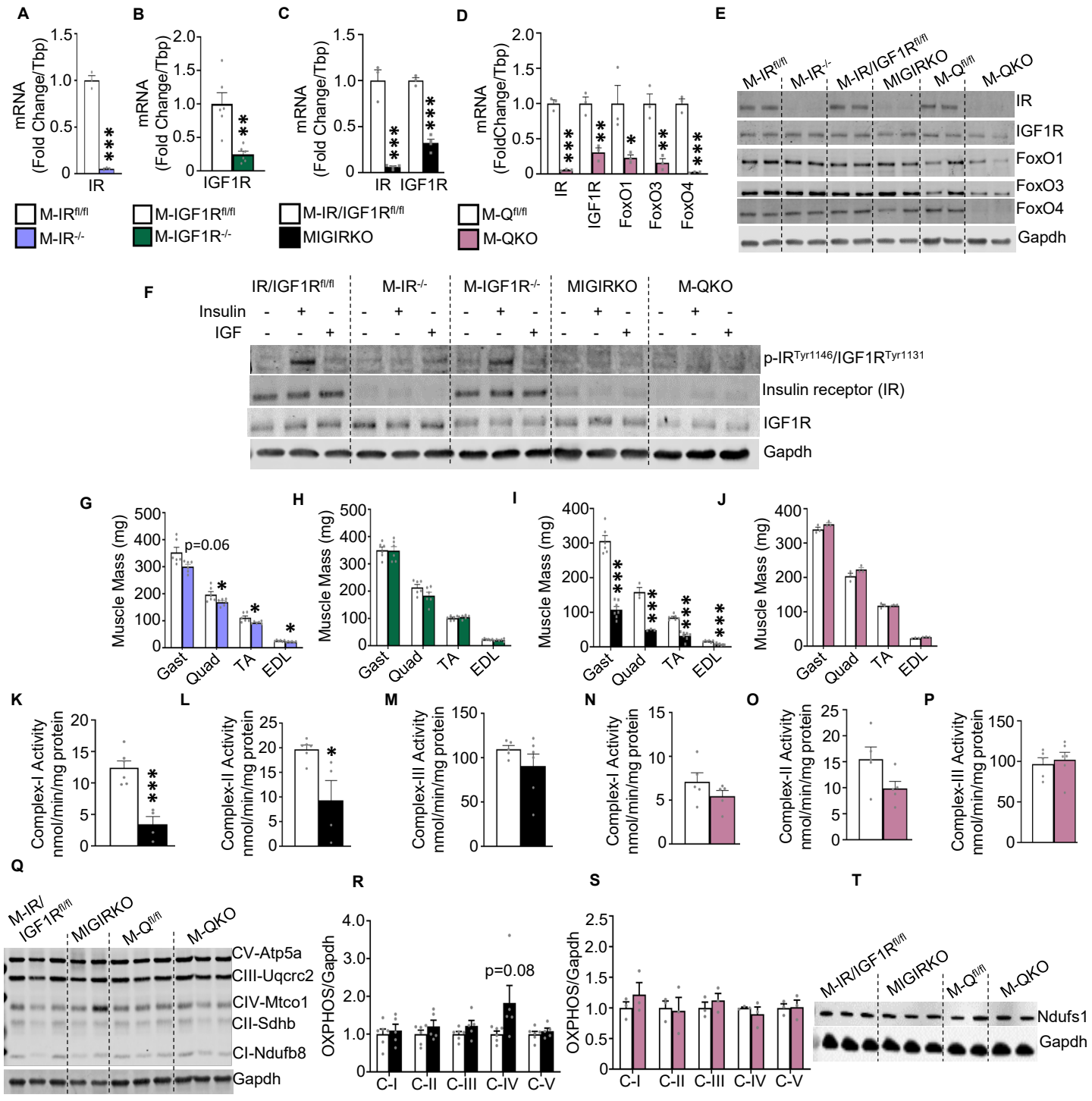

Supplemental Figure 2. Muscle-specific loss of IR alone showed mild decrease in muscle mass, whereas combined deletion of IR and IGF1R induces dramatic decline in muscle mass and OXPHOS complex-I activity, and these abnormalities are not present in M-QKO muscle. (A-D) mRNA level of specified genes in soleus quantified using qPCR in M-IR$^{-/-}$ (A), M-IGF1R$^{-/-}$ (B), MIGIRKO (C), and M-QKO (D) with respective controls (n=3-6). Tbp (TATA-Box Binding Protein) is used as a normalizer for total mRNA.**(E)** Western blot of IR, IGF1R, FoxO1, FoxO3, and FoxO4 in soleus from M-IR$^{-/-}$, MIGIRKO, and M-QKO with respective floxed controls (n=2). **(F)** Western blot of p-IR/IGF1R, IR and IGF1R in soleus from M-IR$^{-/-}$, M-IGF1R$^{-/-}$, MIGIRKO, M-QKO, and M-IR/IGF1R$^{fl/fl}$ mice treated with either insulin and/or IGF-1. **(G-J)** Muscle mass in M-IR$^{-/-}$ (G), M-IGF1R$^{-/-}$ (H), MIGIRKO (I), and M-QKO (J) with respective controls (n=3-6). **(K-M)** OXPHOS complex-I (K), complex-II (L), and complex-III (M) activity in quad from MIGIRKO and M-IR/IGF1R$^{fl/fl}$ (n=4-6). **(N-P)** Complex-I (N), complex-II (O), and complex-III (P) activity in quad from M-QKO and M-Q$^{fl/fl}$ (n=4-6). **(Q-S)** Western blot image (Q) of OXPHOS proteins and densitometry in quad from MIGIRKO (R), and M-QKO (S) with their respective controls (n=3-6). **(T)** Western blot of Ndufs1 in quad from MIGIRKO and M-QKO with respective controls (n=2-3). Results represented as the mean ± SEM. (*P < 0.05, **P < 0.01, ***P < 0.001 vs. littermate control, t-test for 2 groups).

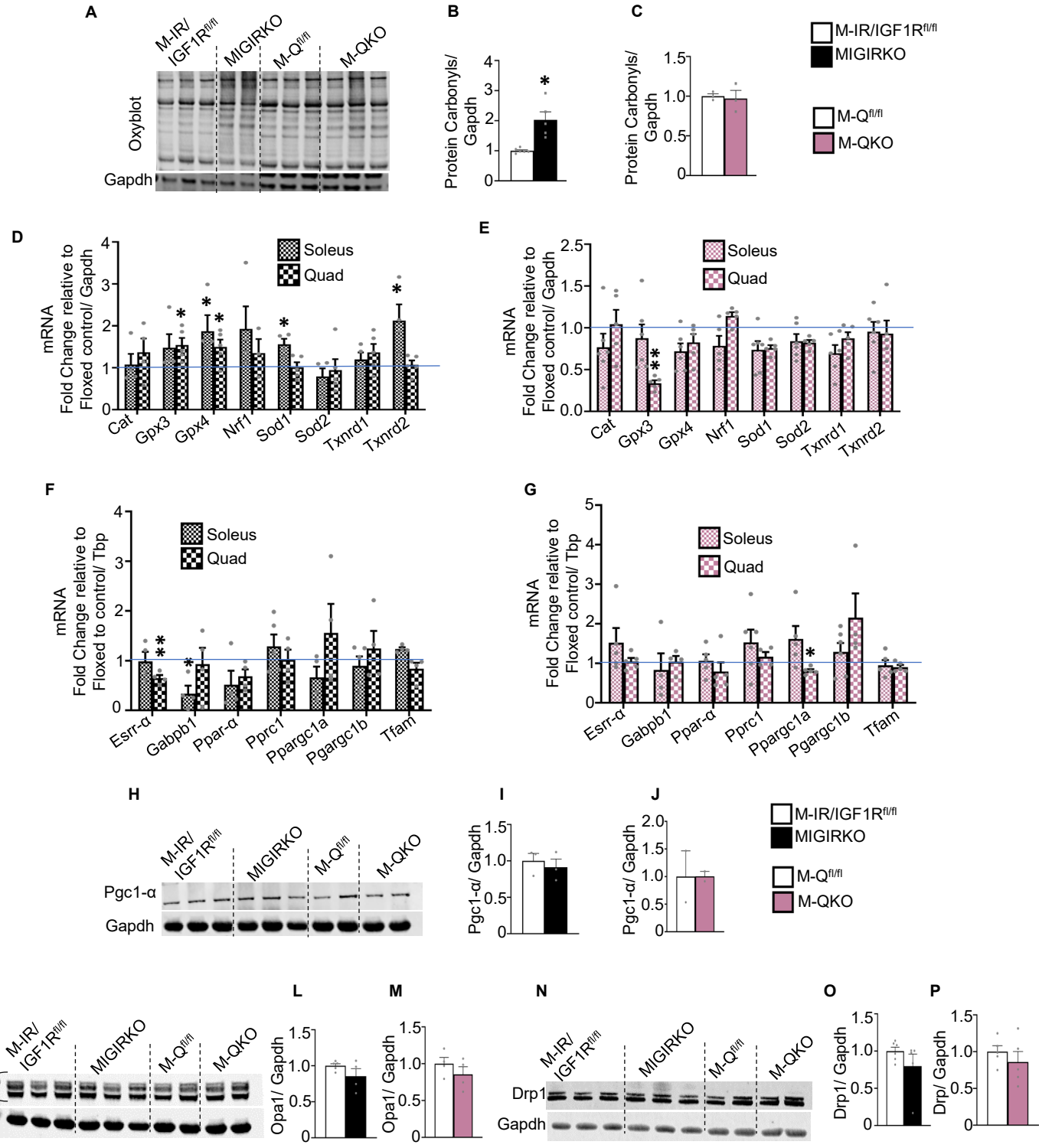

Supplemental Figure 3. Protein carbonylation and antioxidant genes were increased in MIGIRKO and normalized in M-QKO, whereas mitochondrial biogenesis genes and fission-fusion proteins were unchanged both in MIGIRKO and M-QKO muscle. Representative image of Oxyblot (A) and densitometry in quad from MIGIRKO (B), and M-QKO (C) with respective controls (n=3-6). **(D** and **E)** qPCR of antioxidant genes in soleus and quad from MIGIRKO (D) and M-QKO (E) presented as fold-change relative to their respective floxed controls (n=4-5) normalized with Gapdh. **(F** and **G)** qPCR of mitochondrial biogenesis genes in soleus and quad from MIGIRKO (F) and M-QKO (G) with respect to their respective controls (n=4-6). **(H-J)** Western blot image (H) and densitometry of Pgc1-α in quad from MIGIRKO (I) and M-QKO (J) with respective controls (n=2-3). **(K-M)** Western blot image of fusion protein Opa1 (K) and densitometry in quad from MIGIRKO (L) and M-QKO (M) with littermate controls (n=4-5). **(N-P)** Western blot image (N) and densitometry of fission protein Drp1 in quad from MIGIRKO (O) and M-QKO (P) with littermate controls (n=2-5). Results represented as the mean ± SEM. (*P < 0.05, **P < 0.01 vs. littermate control, t-test for 2 groups)

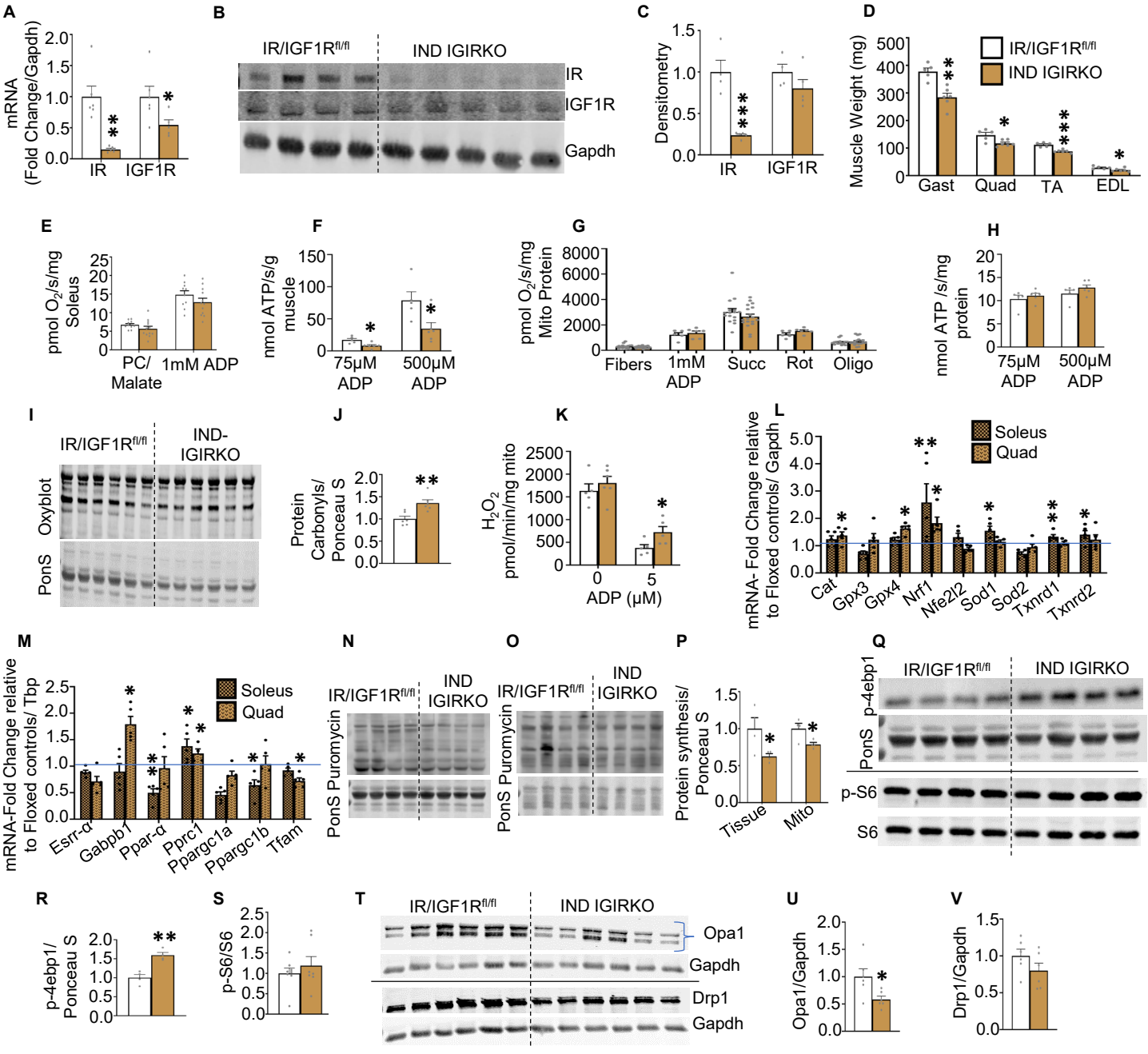

Supplemental Figure 4. Tamoxifen-inducible deletion of IR and IGF1R in muscle decreases muscle mass, protein synthesis and fusion protein Opa-1, while increasing H_2O_2, protein carbonylation, antioxidant genes and mTOR signaling. (A) mRNA level of IR and IGF1R quantified using qPCR in quad 21 days after tamoxifen-treatment in IND-IGIRKO and IR/IGF1R$^{fl/fl}$ mice. **(B** and **C)** Western blot (B) and densitometry (C) of IR and IGF1R in quad from IND-IGIRKO. **(D)** Muscle weight on day 21 after tamoxifen treatment in IND-IGIRKO and IR/IGF1R$^{fl/fl}$ (n=5-6). **(E** and **F)** Respiratory capacity in permeabilized soleus fibers (E), and ATP synthesis rate (F) with PC and malate from IND-IGIRKO and IR/IGF1R$^{fl/fl}$ (n=5-12). **(G)** Respiration in mitochondrial isolates from quad/gast with glutamate and malate, then with subsequent addition of ADP, succinate, rotenone, and oligomycin from IND-IGIRKO (n=5-16). **(H)** ATP synthesis in mitochondria from IND-IGIRKO with glutamate and malate (n=5-6) at low 75 μM and high 500 μM ADP concentration. **(I** and **J)** Oxyblot image showing carbonylation on proteins (I) with densitometry (J) in quad from IND-IGIRKO (n=6). **(K)** H_2O_2 production in mitochondrial isolates from quad/gast (n=5-6). **(L)** qPCR of antioxidant genes in soleus and quad from IND-IGIRKO shown as fold change of IR/IGF1R$^{fl/fl}$ (n=5-6). **(M)** qPCR of mitochondrial biogenesis genes in soleus and quad from IND-IGIRKO (n=4-6). **(N-P)** Western blot of puromycin incorporation to measure protein synthesis using SUnSET method in quad tissue homogenate (N) and mitochondrial isolates from quad/gast (O) with densitometry (P) in IND-IGIRKO and controls (n=4). **(Q-S)** Western blot (Q) and densitometry of p-4ebp1 (R), and p-S6 (S) in quad from IND-IGIRKO and IR/IGF1R$^{fl/fl}$ (n=4-8). **(T-V)** Western blot image (T) and densitometry of Opa1 (U) and Drp1 (V) in quad from IND IGIRKO and IR/IGF1R$^{fl/fl}$ (n=6). Results represented as the mean ± SEM. (*P < 0.05, **P < 0.01, ***P < 0.001 vs. littermate control, t-test for 2 groups)

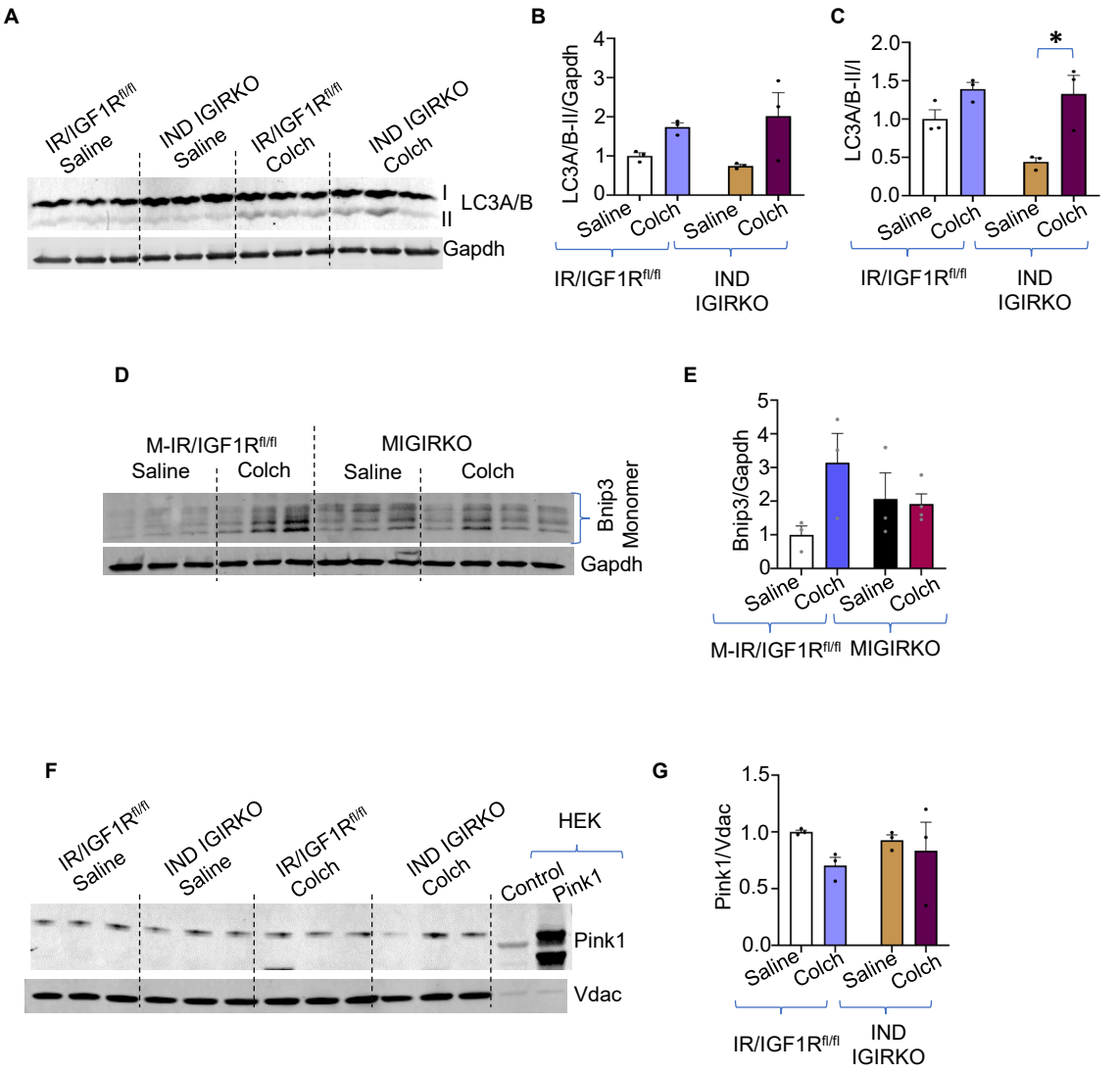

Supplemental Figure 5. Mitophagy flux is not activated in MIGIRKO and IND-IGIRKO muscle. (A-C) Western blot image (A) of LC3A/B and densitometry of LC3A/B-II (B), and ratios of LC3AB-II/I (C) in quad tissue homogenate from IND-IGIRKO and IR/IGF1R$^{fl/fl}$ treated either with colchicine or saline (n=3). **(D** and **E)** Western blot image (D) from MIGIRKO with densitometry (E) of Bnip3 in quad after colchicine treatment (n=3-4). **(F** and **G)** Western blot (F) and densitometry (G) of Pink1 in quad/gast mitochondrial isolates from IND-IGIRKO and IR/IGF1R$^{fl/fl}$ treated with colchicine or saline (n=3). HEK 293 cells either mock transfected or transfected with tagged PINK1 were used to verify the antibody). Results represented as the mean ± SEM. (*P < 0.05 vs littermate control, t-test for 2 groups)

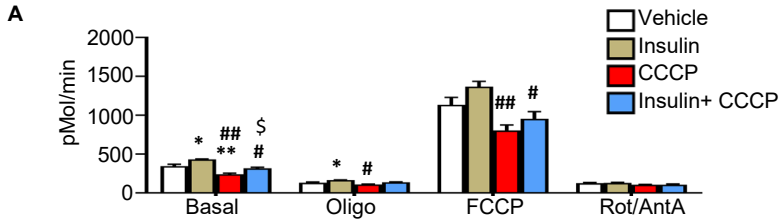

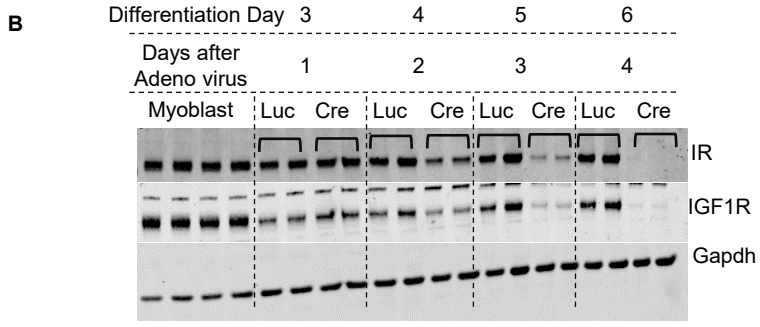

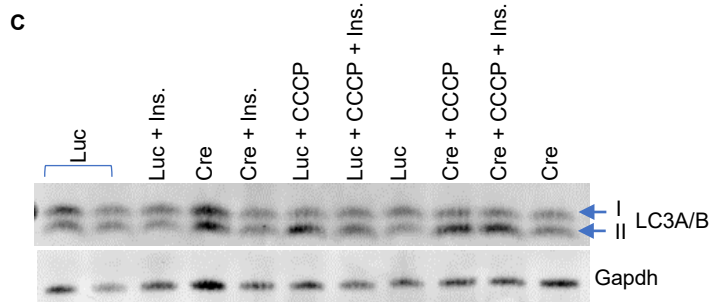

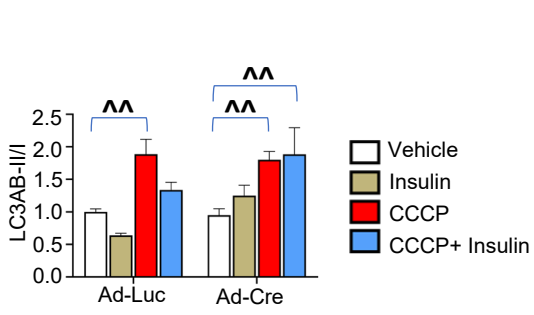

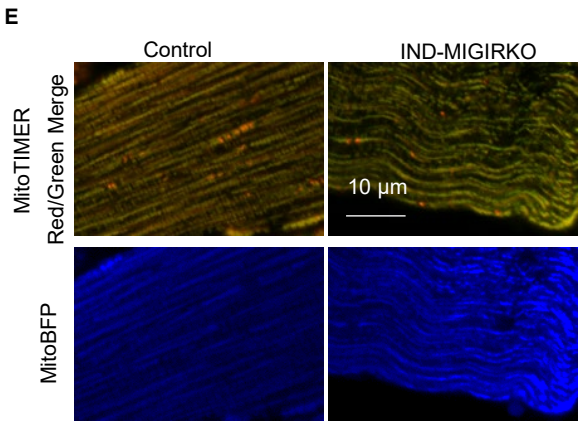

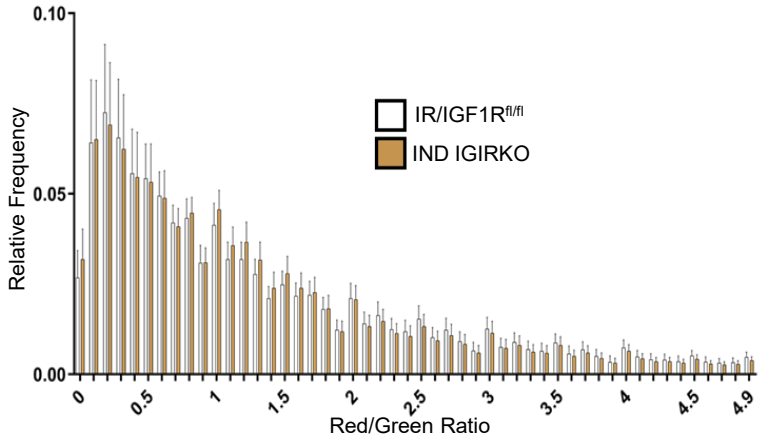

Supplemental Figure 6. Insulin rescues basal respiration dysfunction, induced by CCCP in C2C12 myotubes. **(A)** Oxygen consumption rate (OCR) measured using Seahorse XF24 in C2C12 myotubes treated with or without insulin or pretreated with the mitophagy inducer CCCP (Carbonyl cyanide m-chlorophenylhydrazone) and subsequent washout prior to Seahorse analysis (n=3 experiments). **(B)** Western blot of IR and IGF1R from primary myoblasts and myotubes after treatment of Adenoviral-Cre (Ad-Cre) or Adenoviral-Luciferase (Ad-Luc) **(C** and **D)** Western blot image (C) and densitometry ratio of LC3AB-II/I (D) in primary myotubes treated with Adenoviral-Cre (Ad-Cre) or Adenoviral-luciferase (Ad-Luc) in presence or absence of Insulin (Ins), CCCP, and insulin with CCCP (n=3 experiments). **(E)** Merged image of red and green from mitoTIMER with mitoBFP showing adequate localization of proteins in mitochondria after co-electroporation into TA muscle from IND-IGIRKO and IR/IGF1R$^{fl/fl}$ (Images at 40X) **(F)** Distribution of Red/Green ratio of MitoTIMER fluorescence measured in each pixel with fluorescent signal in TA from IND-IGIRKO and IR/IGF1R$^{fl/fl}$ (n=9-10). Results represented as the mean ± SEM. (*P < 0.05, **P < 0.01 vs. control, #P < 0.05 and ##P < 0.01 vs insulin, $ P, 0.05 vs CCCP, Two-way ANOVA) (^^P<0.01 vs. vehicle, Three-way ANOVA). (B-Blots are from parallel samples run on separate gels). (Disclosures-A subset of the lanes in supplemental figure 6B are also shown in figure 6G. Additionally, merged panels from figure 6I are presented in supplemental figure 6E)

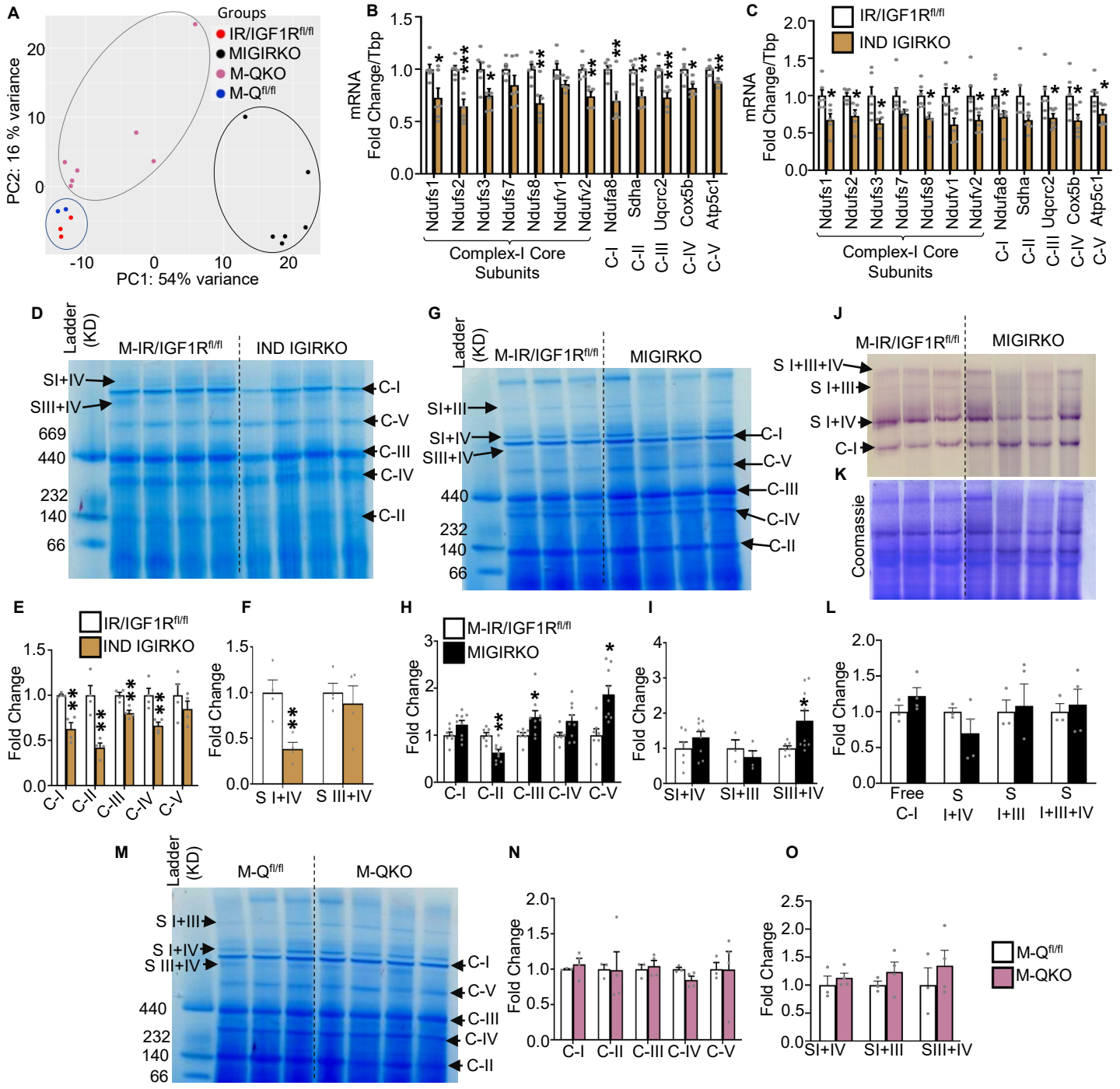

Supplemental Figure 7. OXPHOS complex-I subunit mRNAs, and complex-I driven supercomplex formation is decreased in IND-IGIRKO, whereas minimal changes in OXPHOS are seen in MIGIRKO and M-QKO muscle. (A) Principal component analysis (PCA) plot from RNA-Seq in MIGIRKO and M-QKO muscle with respective fl/fl controls. **(B** and **C)** qPCR of selected genes of OXPHOS subunits from soleus (B), and quad (C) in IND-IGIRKO and IR/IGF1R$^{fl/fl}$ (n=5-6). **(D** and **F)** Representative image of blue native gel (D), with densitometry of OXPHOS complex I-V (E) and supercomplexes (F) in soleus muscle from IND-IGIRKO and IR/IGF1R$^{fl/fl}$ (n=5-6). **(G-I)** Representative image of blue native gel (G) in quad with densitometric analysis of OXPHOS complex (H), and supercomplexes (I) from MIGIRKO and M-IR/IGF1R$^{fl/fl}$ (n=8-9). **(J-L)** Representative image showing complex-I in-gel activity (J) with Coomassie stain (K), and densitometry (L) in quad from MIGIRKO and M-IR/IGF1R$^{fl/fl}$ (n=3-4). **(M-O)** Representative image of blue native gel (M) in homogenates from quad with densitometry of OXPHOS complex (N), and supercomplexes (O) from M-QKO and M-Q$^{fl/fl}$ (n=3-4). Results represented as the mean ± SEM. (*P < 0.05, **P < 0.01, ***P < 0.001 vs. littermate control, t-test for 2 groups).

SUPPLEMENTAL METHODS

Animal Models

This study included various muscle-specific knock out mouse lines (M-IR$^{-/-}$, M-IGF1R$^{-/-}$, MIGIRKO, M-FoxO TKO, M-QKO, and IND-IGIRKO), and each knock out line was bred independently so that all targets for knockout were on a "double floxed" colony if able. The one exception is that the MIGIRKO mice are infertile so Acta1-Cre, IR$^{fl/+}$IGF1R$^{fl/fl}$ were bred to IR$^{fl/fl}$IGF1R$^{fl/fl}$. To generate MIGIRKO, M-IR$^{-/-}$ and M-IGF1R$^{-/-}$ mouse lines, the initial cross between an Acta1-Cre mouse (stock 006149; Jackson Laboratory) and an IR$^{fl/fl}$IGF1R$^{fl/fl}$ mouse were crossed in 2011. The F1 generation was intercrossed and breeders from the F2 generation were selected to obtain the three colonies M-IR$^{-/-}$ (Acta1-cre, IR$^{fl/fl}$), M-IGF1R$^{-/-}$ (Acta1-cre, IGF1R$^{fl/fl}$), and MIGIRKO (Acta1-cre, IR$^{fl/fl}$, IGF1R$^{fl/fl}$). These mice were extensively characterized for muscle mass and glucose homeostasis (1, 2). In 2013, muscle quintuple knockout and FoxO TKO mice were created by crossing to a Acta1-Cre, IR$^{fl/+}$IGF1R$^{fl/fl}$ mouse from the MIGIRKO colony to FoxO1$^{fl/fl}$FoxO3$^{fl/fl}$FoxO4$^{fl/fl}$ mouse. MIGIRKO was re-derived from this by crossing back to IR$^{fl/fl}$IGF1R$^{fl/fl}$ while FoxO TKO and M-QKO were derived by crossing back to FoxO1$^{fl/fl}$FoxO3$^{fl/fl}$FoxO4$^{fl/fl}$, then selecting for breeders from this F2 generation, which were again well studied for proteostasis and muscle atrophy (2). All animals were on a mixed background containing C57Blk6, C57Blk6J, and 129 strains and as such may contain random mutations in the Nnt (Nicotinamide nucleotide transhydrogenase) gene. A post-hoc determination of Nnt genotype revealed that MIGIRKO and M-IR/IGF1R$^{fl/fl}$ were heterozygous, whereas other strains (M-IR$^{-/-}$, M-IR$^{fl/fl}$, M-QKO, and M-Q$^{fl/fl}$) were mixed homozygous and heterozygous for Nnt gene (data not shown), but did not correlate with the mitochondrial differences demonstrated in our study.

Given the mixed background of the initial founders (C57Blk6, C57Blk6J, and 129 strains) and multiple crosses needed to generate these mice, we acknowledge that genomic heterogeneity is a limitation of the study. Importantly, each knockout is compared with their respective littermate single or double floxed controls. Thus for the current study, to minimize genetic heterogeneity, M-IR$^{-/-}$ mouse line is compared with M-IR$^{fl/fl}$ controls, M-IGF1R$^{-/-}$ is compared with M-IGF1R$^{fl/fl}$, MIGIRKO is compared with M-IR/IGF1R$^{fl/fl}$ and/or M-IR/IGF1R$^{fl/+}$, M-FoxO TKO is compared with M-FoxO T$^{fl/fl}$ (abbreviated T$^{fl/fl}$), and M-QKO is compared with M-Q$^{fl/fl}$ controls. Similarly, tamoxifen induced IR/IGF1R knock out (IND- IGIRKO) animals were compared with tamoxifen treated IR/IGF1R$^{fl/fl}$ controls. To minimize the genetic and experimental variation, for every experiment, a cohort of knock out animals and their respective controls were euthanized on the same day and time, and mitochondrial functional studies, biochemical assays and molecular biology experiments were performed.

Isolation of Mitochondria and Mitochondrial Respiration

Muscle mitochondria used in all functional experiments including respiratory experiments and H_2O_2 assays, was isolated using differential centrifugation from the mixture of one entire quadriceps and one entire gastrocnemius muscle using the method as described previously with minor modifications (3). Briefly, freshly extracted muscle (1 quad and 1 gastroc from each animal to minimize variability due to fiber type composition) was immediately minced into small

pieces, and washed twice in ice-cold PBS buffer supplemented with 10 mM EDTA. Minced tissue was digested for 30 min in 5ml of ice-cold PBS mixed with 10mM EDTA and 0.05% trypsin, then centrifuged at 200g for 5 min and the collected supernatant was discarded. Tissue pieces were resuspended in 4ml of IBm1 buffer (1 M sucrose, 1 M Tris/HCl, 1 M KCl, 1M EDTA, and 10% BSA, pH-7.4), and homogenized in ice using motor-driven glass homogenizer. Homogenate was then centrifuged at 700g for 10 min at 4^0C, supernatant was collected, and again centrifuged at 8000g for 10 min. The pellet was resuspended in 1ml of IBm2 buffer (1 M sucrose, 0.1 M EGTA/Tris and 1 ml of 1 M Tris/HCl, adjust pH to 7.4), split into 2 parts, and centrifugation at 8000g for 10 min. Supernatant was discarded, and the final mitochondrial pellet was dissolved either in "respiration buffer" (120 mmol/L KCl, 5 mmol/L KH_2PO_4, 2 mmol/L $MgCl_2$, 1 mmol/L EGTA, 3 mmol/L HEPES [pH 7.2] with 0.3% fatty acid–free BSA) (4) for respiration and H_2O_2 assays, or RIPA buffer for western blot analysis.

For initial experiments in $T^{fl/fl}$, STZ diabetic $T^{fl/fl}$, M-FoxO TKO, STZ-FoxO TKO, M-$IR^{fl/fl}$, and M-$IR^{-/-}$, we determined mitochondrial respiration in isolated mitochondria using "respiration buffer", but could not measure ATP synthesis in this buffer. Thus, all subsequent isolated mitochondrial respiration experiments were performed in modified buffer Z, which contained 0.5 mg/ml BSA instead of 2.5 mg/ml BSA and did not contain blebbistatin or creatine monohydrate (full list of chemicals and concentrations: 105 mM K-MES, 30 mM KCl, 10 mM KH_2PO_4, 5 mM $MgCl_2$-$6H_2O$, 0.5 mg/ml BSA, 1 mM EGTA, pH 7.4). Mitochondrial respiration data from $T^{fl/fl}$, STZ diabetic $T^{fl/fl}$, M-FoxO TKO, STZ-FoxO TKO using either respiration buffer or modified buffer Z were combined as a fold change of $T^{fl/fl}$ in Figure 1A.

In vivo Insulin Signaling Measurement

In vivo insulin and IGF-1 signaling was determined in anesthetized, six-hour fasted mice by injecting either regular insulin (5U Relion brand Novolin R) or 1 mg/kg recombinant human IGF-1 (Fisher scientific # 291G1200) via inferior vena cava (IVC). Ten minutes later muscle tissue was harvested, snap frozen in liquid nitrogen, and immediately stored in -80^0C for further processing.

Transmission Electron Microscopy

Electron microscopy was performed in conjunction with the University of Iowa Central Microscopy Research Facility . Briefly, soleus muscle was cut into small pieces (~1 mm^3) and fixed in 2.5 % glutaraldehyde solution at 4^0C until further processing. Tissue was post fixed in 1% osmium tetroxide (OsO_4) and 1.5% potassium ferrocyanide in 0.2 M cacodylate buffer for 1.5 hour at room temperature. Muscle pieces were then stained with 2.5 % uranyl acetate for 20 min, dehydrated with a series of ethanol dilutions (50-100%), and embedded in EPON resin. Embedded tissue was sectioned using Leica UC6 ultramicrotome, and ultrathin sections were mounted on grids, contrasted with uranyl acetate and lead citrate, and observed in the JEOL JEM-1230 Transmission Electron Microscope. Images of intermyofibrillar mitochondria were obtained from uniform areas near a peripheral nucleus and analyzed using a grid technique in a blinded fashion (5).

Treadmill and Grip-Strength Test

IND-IGIRKO muscle exercise capacity was determined using treadmill exhaustion test on motor-driven treadmill (Columbus Instruments) as previously described with minor modifications (6). Briefly, for 2 days, mice were acclimated for running on treadmill with an electric shock grid. On the first day, treadmill speed was set at 5 m/min for 30 min, and on the second day two rounds of 15 min cycles (12 min at 5m/min, and 3 min at 10m/min speed) were performed. On the third day, exercise tolerance was tested with a speed of 4m/min, and thereafter speed was increased by 2 m/min in every 10 min. Running was terminated when mice were unable to get off the electrified grid for 10s.

Forelimb grip strength was measured in IND-IGIRKO and control mice using a triangular pull bar attached to a grip strength meter (Columbus Instruments), as described previously (6).

Citrate Synthase and OXPHOS complex Activity Assays

Citrate synthase (CS) activity was assessed either in soleus, quadriceps or gastrocnemius muscle, according to the protocol described previously (7, 8). In brief, muscle was homogenized in a buffer containing 250 mM sucrose, 20 mM tris, 40 mM KCl, and 2 mM EGTA at pH 7.4. CS reaction was performed with 5 µg protein lysate in a final solution of 200 µl containing 200 mM tris with a pH of 8.0, 0.2% v/v Triton X-100, 100 µl of 5,5'-Dithiobis (2-nitrobenzoic acid), 10 mM Acetyl-CoA, and 0.5 mM oxaloacetic acid. Reaction was monitored at 412 nm for 3 min using spectrophotometer.

Mitochondrial respiratory chain complex I, II, and III activities were measured either in quadriceps, gastrocnemius, or soleus muscle according to the method described previously (7). In brief, muscle was homogenized as described above in CS assay. Activity of complex-I was performed using 40 µg protein lysate for quad or gast, or 10 µg for soleus, in a final solution of 200 µl complex-I assay buffer (0.5 M potassium phosphate (pH 7.5), 50 mg/ml fatty-acid free BSA, 10 mM KCN, and 10 mM NADH) with and without complex-I inhibitor 1 mM rotenone. Reaction was started with the addition of 10 mM ubiquinone, and absorbance was monitored spectrophotometrically at 340 nm for 10 min. For complex-II activity, 10 µg protein lysate (5 µg for soleus) was mixed with 200 µl complex-II buffer (0.5 M potassium phosphate (pH 7.5), 50 mg/ml fatty-acid free BSA, 10 mM KCN, and 400 mM succinate) with and without 1 M malonate, and baseline absorbance was measured initially using spectrophotometer at 600 nm for 5 min. Reaction was started with the addition of 12.5 mM decylubiquinone, and monitored again at 600 nm for 10 min. Complex-III activity was performed using 3 µg protein lysate in 200 µl complex-III buffer containing 0.5 M potassium phosphate (pH 7.5), 75 µl of oxidized cytochrome c, 10 mM KCN, 5 mM EDTA, 2.5 % v/v tween-20 with and without complex-III inhibitor 10 mg/ml Antimycin A. Absorbance was monitored at baseline, and after addition of 10 mM decylubiquinol at 550 nm for 2 min.

Cellular Systems, Transfection, and Adenoviral Construct Preparation

In vitro studies were performed using C2C12 or IR/IGF1R floxed myoblast cell lines on day 7 of differentiation.

We transfected Pink1 (Addgene, Catalogue # 13320) plasmid in HEK cells using DNA Transfection Reagent (Bimake, Cat# B35101), and the overexpressed Pink1 protein in Human embryonic kidney (HEK) cells was used as a positive control in Pink1 western blot experiments.

Induction of mitophagy by loss of IR/IGF1R was performed in primary myotubes using Adenoviral-mitoKeima which we generated using Gateway system (Thermofisher). Plasmid pIND-mt mKeima (mitoKeima) was kindly provided by Dr. Vitor A. Lira. PCR amplification of the mitoKeima and, in a sperate reaction, pEntr vector was amplified. PCR products of mitoKeima and pEntr were cut with KpnI and EcoR1 (New England Biolabs), ligated using LR clonase II enzyme mix (Invitrogen, Cat. # 11791-020) and transformed into stbl3 competent E. coli bacterial strain using kanamycin agar plates. Colonies were picked and then mitoKeima was ligated into pAd/CMV/V5-Dest using the gateway method (Life technology, cat. 12536-017, and 12535-035) for viral generation in HEK 293 cells followed by purification.

To generate pure adenovirus, pAd-mito-Keima was linearized with PacI and transfected into 80% confluent HEK293 cells using CalFectin (SignaGen Laboratories, Cat # SL100478) and split onto a larger plate the following day. Viral plaques appeared 4-7 days later and were used for 3 rounds of subsequent amplification, resulting in six 15cm dishes with crude virus. Purification involved colleting the cell pellet, resuspension in freezing buffer (10 mM Tris pH 8.0, 1 mM $MgCl_2$), and addition of 10% NP-40. The lysate was spun on a CsCl gradient then desalted to produce purified Ad-mitoKeima virus.

In vitro Mitophagy Assessment Using mt-Keima Biosensor

Adenoviral mitoKeima was used to assess mitophagy in vitro in primary myotubes in which IR/IGF1R were deleted. MitoKeima is a mitochondrial targeted pH sensitive fluorescent protein which changes its excitation from 440 nm to 550 nm when mitochondria fuse with the lysosomes (9, 10). Primary myoblasts with floxed IR/IGF1R were seeded on Matrigel (Life Sciences, product number: 354248) coated plates in growth media (DMEM -F12, 20% fetal bovine serum, 100U/ml PenStrep, and 1X Amphotericin B) supplemented with bFGF (10 ng/ml). When myoblasts were 100% confluent, media was replaced to differentiation media (DMEM -F12, 2% fetal bovine serum, 100U/ml PenStrep, and 1X Amphotericin B). On day 2 of differentiation, myotubes were infected with control Adenoviral- luciferase (Ad-luc) or Adenoviral-Cre (Ad-Cre) to delete IR/IGF1R, along with Adenoviral-mt-Keima (Ad-mt-Keima given to all myotubes) for mitophagy assessment. On day 7 of differentiation, matured myotubes were serum starved for 4 h, and treated with one of the following treatments: Vehicle, 10nM insulin, 10 μM carbonyl cyanide m-chlorophenylhydrazone (CCCP), or insulin + CCCP for 4 h. Images were acquired using inverted microscope (Leica DMI6000) at Excitation/Emission 440/650, and 550/650 nm. Data was analyzed using ImageJ software, and ratios of fluorescence using 550 nm excitation divided by fluorescence with 440nm excitation was calculated for mitophagy assessment.

Mitochondrial function in C2C12 Myotubes

C2C12 myoblasts were seeded in Seahorse XF24 plate and proliferated in growth media (DMEM -high glucose, 10% fetal bovine serum, 100U/ml PenStrep, and 1X Amphotericin B) in

CO_2 incubator at 37^{O}C, and 5% CO_2. When myoblasts were fully confluent, growth media was replaced to low serum containing differentiation media (DMEM -high glucose, 2% horse serum, 100U/ml PenStrep, and 1X Amphotericin B). On the day 7 of serum restriction, matured multinucleated myotubes were treated with or without insulin (10 nM), mitochondrial uncoupler CCCP (10 μM), and insulin + CCCP for 4 h. Myotubes were washed 3 times with PBS to eliminate CCCP before Oxygen Consumption Rate (OCR) measurement in XF24 Seahorse analyzer (Seahorse Bioscience). Manufacturer's protocol was used to run the assays. Briefly, after myotubes were washed to eliminate CCCP, Seahorse assay buffer (DMEM base 8.3g/L, 2mM GlutaMax-1, 1mM sodium pyruvate, 25mM glucose, and 31.66mM NaCl) containing either vehicle or 10 nM insulin was added to cells that had been pretreated and were equilibrated for 1 hour in CO_2 incubator, then placed in analyzer, and OCR was recorded under basal conditions, and after sequential Injection of 1 μg/ml oligomycin, 8 μM FCCP, and 1 μM Rotenone + 5 μM Antimycin A.

Electroporation and *In vivo* mitophagy assessment

In vivo mitophagy was assessed using mitoTIMER, which is a mitochondria-targeted green fluorescent protein, and shifts to red fluorescent when oxidized (11, 12). MitoTIMER (Addgene #52659), LAMP1-YFP (Addgene#1816), and mitoBFP (Addgene#49151) were cultured in DH5α Escherichia coli, grown in LB agar, and then purified using endotoxin-free plasmid DNA purification kit (TaKaRa, Cat. 740424.10). Plasmid constructs were electroporated into TA muscle by somatic gene transfer. Mice were anesthetized (isoflurane) and 1 TA muscle of each mouse was injected with hyaluronidase solution (0.4 mg/ml) subcutaneously. 2 h later mice were anesthetized a second time, and a 25-μg (total volume 30 μl) mixture from mitoTIMER (10 μg), LAMP1-YFP (10 μg), and mitoBFP (5 μg) plasmid dissolved in saline were injected into tibialis anterior (TA) muscle. Immediately after plasmid injections, the legs were exposed to 10 electric pulses (20 ms) of 175 V/cm (with 480 ms intervals between pulses) using an ECM-830 electroporator (BTX, Holliston, MA, USA). Muscle were extracted and fixed 1 week after electroporation, which was 21 days after tamoxifen treatment in these mice, and longitudinal sections were prepared.

Harvested TAs were immediately fixed in 4% paraformaldehyde solution for 48 h at 4^{0}C. Further, fixed muscle ran through a sequence of incubations with sucrose gradient solutions [i.e., 10% (w/v) for 1 h, 20% for 1 h, and 30% overnight] at 4^{0}C, and then embedded in OCT tissue-frozen medium. Cryosections of the OCT blocks were prepared on glass slides using a Microm HM505E cryostat (Microm International, Walldorf, Germany), and images were taken using Zeiss LSM710, confocal microscope (Oberkochen, Germany). Muscle sections on glass slides were mounted with oil, capped with coverslips, and images were acquired at 40X magnification with non-overlapped channels. MitoTimer images were acquired using the green (excitation/emission 488/518 nm) and red (excitation/emission 543/572 nm) channels as described previously. mitoBFP images were acquired using the blue channel (excitation/emission 399/456 nm), whereas LAMP1-YFP images were acquired using the yellow channel (excitation/emission 515/527 nm). Image analysis is described in the Methods section of the main text.

In vivo Protein Synthesis (SUnSET Method)

For *in vivo* measurement of protein synthesis in IND-IGIRKO muscle, SUnSET method was used, as previously described (13). In brief, 0.04 µmol/g puromycin dissolved in PBS was intraperitonially administered 21 days after 5 injections of tamoxifen in IND-IGIRKO and control mice. 30 min after puromycin injections, muscles were extracted and either snap frozen or underwent mitochondrial isolation. Western blotting was performed in muscle homogenate or mitochondrial isolates using anti-puromycin antibody. Peroxidase anti-mouse IgG secondary antibody was used, and chemiluminescent ECL western blotting substrate (Thermo Scientific) was used to develop these blots.

H_2O_2 Measurement

H_2O_2 production was assessed in isolated mitochondria enriched from the mixture of quadriceps and gastrocnemius muscle, as previously described (4). H_2O_2 was measured in 100µg/ml mitochondrial protein mixed in respiration buffer (120 mmol/L KCl, 5 mmol/L KH_2PO_4, 2 mmol/L $MgCl_2$, 1 mmol/L EGTA, 3 mmol/L HEPES [pH 7.2] with 0.3% fatty acid free BSA) supplemented with 5unit/ml Horseradish peroxidase (Sigma P8375) and 20 µM Ampliflu Red (Sigma 90101). Succinate (5 mM), malate (2 mM) and glutamate (10 mM) mixture was used as a substrate for OXPHOS, whereas oligomycin (0.01 mg/ml) was used to inhibit ATP synthase activity. Various ADP concentrations (0-1000 µM) were used to measure H_2O_2 generation. To clamp the ADP concentration at low physiologic levels, 5 mM 2-deoxyglucose and 5 unit/ml Hexokinase were added to the buffer, which constantly utilizes ATP and regenerates ADP, as previously described (4). H_2O_2 reacts with HRP and Ampliflu Red to produce a fluorescent product Resorufin, which was measured in a microplate fluorometric reader at 37^0C with Ex/Em (530 nm/590 nm) for 20 min.

Protein Carbonylation

Oxyblot Protein Carbonyl Assay Kit (Abcam-ab 178020) according to the instructions provided by the manufacturer. In summary, muscle protein was derivatized to 2,4-denitrophenylhydrazone (DNP) by reaction with 2,4-denitrophenylhydrazine (DNPH). These DNP moieties were detected using an anti-DNP antibody in western blotting, and carbonylation on proteins was quantified using densitometry with normalization to total protein by Ponceau S or Gapdh or normalized to Vdac content in mitochondrial fractions.

Autophagy Flux and Mitophagy Flux Analysis

To measure autophagy flux and mitophagy flux**,** an autophagy inhibitor Colchicine (0.4 mg/kg/d; Sigma Aldrich) or saline was intraperitonially administered in mice for 3 days as previously described (14). In IND-IGIRKO mice, colchicine treatment started after 18 days of tamoxifen injections, and 3 injections of colchicine were given. After colchicine treatment, muscles were harvested, and western blotting was performed for selected autophagy and mitophagy markers both in tissue lysate and mitochondrial isolates.

References

1. O'Neill BT, Lauritzen HP, Hirshman MF, Smyth G, Goodyear LJ, and Kahn CR. Differential Role of Insulin/IGF-1 Receptor Signaling in Muscle Growth and Glucose Homeostasis. *Cell Rep.* 2015;11(8):1220-35.
2. O'Neill BT, Lee KY, Klaus K, Softic S, Krumpoch MT, Fentz J, et al. Insulin and IGF-1 receptors regulate FoxO-mediated signaling in muscle proteostasis. *J Clin Invest.* 2016;126(9):3433-46.
3. Frezza C, Cipolat S, and Scorrano L. Organelle isolation: functional mitochondria from mouse liver, muscle and cultured fibroblasts. *Nat Protoc.* 2007;2(2):287-95.
4. Yu L, Fink BD, Herlein JA, and Sivitz WI. Mitochondrial function in diabetes: novel methodology and new insight. *Diabetes.* 2013;62(6):1833-42.
5. O'Neill BT, Kim J, Wende AR, Theobald HA, Tuinei J, Buchanan J, et al. A conserved role for phosphatidylinositol 3-kinase but not Akt signaling in mitochondrial adaptations that accompany physiological cardiac hypertrophy. *Cell Metab.* 2007;6(4):294-306.
6. Dyle MC, Ebert SM, Cook DP, Kunkel SD, Fox DK, Bongers KS, et al. Systems-based discovery of tomatidine as a natural small molecule inhibitor of skeletal muscle atrophy. *J Biol Chem.* 2014;289(21):14913-24.
7. Spinazzi M, Casarin A, Pertegato V, Salviati L, and Angelini C. Assessment of mitochondrial respiratory chain enzymatic activities on tissues and cultured cells. *Nat Protoc.* 2012;7(6):1235-46.
8. Penniman CM, Suarez Beltran PA, Bhardwaj G, Junck TL, Jena J, Poro K, et al. Loss of FoxOs in muscle reveals sex-based differences in insulin sensitivity but mitigates diet-induced obesity. *Mol Metab.* 2019;30:203-20.
9. Katayama H, Kogure T, Mizushima N, Yoshimori T, and Miyawaki A. A sensitive and quantitative technique for detecting autophagic events based on lysosomal delivery. *Chem Biol.* 2011;18(8):1042-52.
10. Sun N, Malide D, Liu J, Rovira, II, Combs CA, and Finkel T. A fluorescence-based imaging method to measure in vitro and in vivo mitophagy using mt-Keima. *Nat Protoc.* 2017;12(8):1576-87.
11. Laker RC, Xu P, Ryall KA, Sujkowski A, Kenwood BM, Chain KH, et al. A novel MitoTimer reporter gene for mitochondrial content, structure, stress, and damage in vivo. *J Biol Chem.* 2014;289(17):12005-15.
12. Laker RC, Drake JC, Wilson RJ, Lira VA, Lewellen BM, Ryall KA, et al. Ampk phosphorylation of Ulk1 is required for targeting of mitochondria to lysosomes in exercise-induced mitophagy. *Nat Commun.* 2017;8(1):548.
13. Schmidt EK, Clavarino G, Ceppi M, and Pierre P. SUnSET, a nonradioactive method to monitor protein synthesis. *Nat Methods.* 2009;6(4):275-7.
14. Ju JS, Varadhachary AS, Miller SE, and Weihl CC. Quantitation of "autophagic flux" in mature skeletal muscle. *Autophagy.* 2010;6(7):929-35.

Supplemental Table 1. Antibodies used for western blots.

Protein	Vendor	Catalog Number	Dilution
p-AKT (Ser473)	Cell Signaling	9271	1:1000
AKT	Cell Signaling	4685	1:1000
Bnip3	Cell Signaling	3769	1:1000
Drp1 (DNM1L)	Abnova	H00010059-M01	1:1000
FoxO1	Cell Signaling	2880	1:1000
FoxO3	Cell Signaling	12829	1:1000
FoxO4	Abcam	128908	1:1000
Gapdh	Cell Signaling	5174	1:1000
p-IR/IGF1R	Cell Signaling	3021	1:1000
IR (Insr)	Cell Signaling	3025	1:1000
IGF1-R	Cell Signaling	3027	1:1000
LC3A/B	Cell Signaling	12741	1:1000
Ndufs1	Abcam	ab102552	1:1000
Opa-1	BD Biosciences	612607	1:1000
OXPHOS	Abcam	ab110413	1:1000
p-4ebp1 (Thr37/46)	Cell Signaling	2855	1:1000
Pgc1-α	Santa Cruz	SC-517380	1:500
Pink1	Novus Biologicals	BC100-494	1:1000
p-S6 (Ser235/236)	Cell Signaling	2211	1:1000
S6	Cell Signaling	2317	1:1000
Vdac	Cell Signaling	4866S	1:1000
Anti-puromycin	University of Iowa (DSHB)	PMY-2A4	1:100
Rabbit secondary antibody	Thermo Fisher	SA5-35571	1:10,000
Mouse secondary antibody	Thermo Fisher	SA5-35521	1:10,000
Peroxidase Anti-mouse IgG (Secondary Ab)	Jackson ImmunoResearch Laboratories	115-035-208	1:10,000

Supplemental Table 2. Primers for quantitative RT-PCR of mouse genes.

Gene name	Forward Primer	Reverse Primer
Atp5c1	CCAGGAGACTGAAGTCCATCA	AGAACCTGTCCCATACACTCG
Bnip3	CCCAGACACCACAAGATACCAACA	GGTCGACTTGACCAATCCCATATCCA
Bnip3l	CACCACAAGAAGATGGGCAGATCA	TGGACCAGTCTGATACCCAGT
Cat	GGAGGCGGGAACCCAATAG	GTGTGCCATCTCGTCAGTGAA
Cox5b	GGAAGACCCTAATCTAGTCCCG	GTTGGGGCATCGCTGACTC
Esrra	CAGCTGTACTCGATGCTCCC	AGCTCTCTACCCAAACGCCT
Foxo1	TGCTGTGAAGGGACAGATTG	GAGTGGATGGTGAAGAGCGT
Foxo3	ACAAACGGCTCACTTTGTCCCAGA	TCTTGCCCGTGCCTTCATTCT
Foxo4	GGTGCCCTACTTCAAGGACA	AGCTTGCTGCTGCTATCCAT
Gabarapl1	GTCATCGTGGAGAAGGCTCCTAAA	GGAGGGATGGTGTTGTTGACAAAG
Gabpb1	TCTGTGGATGGTGCAATTCAG	CACACCGGGTATAAGGCTCC
Gapdh	TGTCGTGGAGTCTACTGGTGTCTT	TCTCGTGGTTCACACCCATCACAA
Gpx3	CCCTTAGTGCATTCAGGCTTAG	AGTGGACAGAGTGAGAGGATAG
Gpx4	CCGATATGCTGAGTGTGGTTTA	GGCTGCAAACTCCTTGATTTC
Insr (IR)	AAATGCAGGAACTCTCGGAAGCCT	ACCTTCGAGGATTTGGCAGACCTT
Igf1r	ATCGCGATTTCTGCGCCAACA	TTCTTCTCTTCATCGCCGCAGACT
Map1lc3b (LC3B)	CACTGCTCTGTCTTGTGTAGGTTG	TCGTTGTGCCTTTATTAGTGCATC
Ndufa8	GAACTTCTTCAGGCAGATAAAGAG	TGCATGTTGGAGTAATCAAGG
Ndufs1	TGCAAATCCCTCGATTCTGTTAC	GCTTTCTCAATCTCTACCAGGC
Ndufs2	TCGTGCTGGAACTGAGTGGA	GGCCTGTTCATTACACATCATGG
Ndufs3	CTGTGGCAGCACGTAAGAAG	GCTTGTGGGTCACATCACTCC
Ndufs7	ACCACTACTCCTACTCGGTTG	GTTCACGCTTGATCTTCCGTT
Ndufs8	GTGGCGGCAACGTACAAGTAT	GAATCCGAGCTGCATTGTCAG
Ndufv1	GTGCGGGTATCTGTGCGTT	GGTTGGTAAAGATCCGGTCTTC
Ndufv2	GGCTACCTATCTCCGCTATGA	TCCCAACTGGCTTTCGATTATAC
Nfe2l2	TCTATGTCTTGCCTCCAAAGG	CTCAGCATGATGGACTTGGA
Nrf1	CGGAAACGGCCTCATGTGT	CGCGTCGTGTACTCATCCAA
Ppargc1a	CCCTGCCATTGTTAAGACC	TGCTGCTGTTCCTGTTTTC
Ppargc1b	CTTGGCTGCGCTTACGAAGA	GAAAGCTCGTCCACGTCAGAC
Ppara	CAGTGGGGAGAGAGGACAGA	AGTTCGGGAACAAGACGTTG
Pprc1	TGGACGCCTCCCTTATATCCC	TGTGAGCAGCGACATTTCATTC
Sdha	GCTTGCGAGCTGCATTTGG	TGTGATCGGGTAGGAAAGAGC
Sod1	TACTGATGGACGTGGAACCC	GAACCATCCACTTCGAGCA
Sod2	GCTTGATAGCCTCCAGCAAC	ACTGAAGTTCAATGGTGGGG
Tbp	ACCCTTCACCAATGACTCCTATG	TGACTGCAGCAAATCGCTTGG
Tfam	TCCAAGCCTCATTTACAAGC	CCAAAAAGACCTCGTTCAGC
Txnrd1	AAGTGGGTGAGATGGCTTATG	GGAGACAATGCTACACCAGTTA
Txnrd2	CACAGGTGATGCAGACAGTAG	CTCAGCAACCAGTCACAGTAG
Uqcrc2	GATAACCCGTGGGATTGAAGC	TCTACAGTGTACGCCATGTTTTC

Supplemental Table 2 (continued). Primers for plasmid amplification.

Gene name	Forward Primer	Reverse Primer
Mt-Keima	GATCGGTACCATGTCCGTCCTGACGCC	GATCGAATTCTTAGCCCAGCAGGG AGT

Supplemental Table 3. Sequence counts and False Discovery Rates (FDR) of OXPHOS genes in MIGIRKO and M-QKO

**-FDR<0.01 MIGRKO vs. Floxed ##-FDR<0.01 MIGIRKO vs. M-QKO

***-FDR<0.001 ###-FDR<0.001

OXPHOS	Symbol		Log2 Sequence counts			MIGIRKOvsFloxed FDR		QKOvsFloxed FDR	QKOvsMIGIRKO FDR	
			Floxed	MIGIRKO	QKO					
	mt-Nd1	ENSMUSG00000064341	13.6	12.7	13.5	0.000282	***	0.858	0.000446	###
	mt-Nd2	ENSMUSG00000064345	12.6	11.40	12.50	0.0000607	***	0.913	0.000063	###
	mt-Nd3	ENSMUSG00000064360	9.87	9.01	6.96	0.51		0.166	0.125	
	mt-Nd4	ENSMUSG00000064363	11.8	10.80	11.70	0.000583	***	0.961	0.000533	###
	mt-Nd4l	ENSMUSG00000065947	1.5	0.61	0.95	0.374		0.712	0.900	
	mt-Nd5	ENSMUSG00000064367	12.9	11.90	13.00	0.000108	***	0.825	0.000025	###
Complex-I	mt-Nd6	ENSMUSG00000064368	10	9.09	10.10	0.000657	***	0.903	0.000223	###
Core subunits	Ndufs1	ENSMUSG00000025968	5.81	5.45	5.99	0.000000164	***	0.573	0.033	
	Ndufs2	ENSMUSG00000013593	7.97	7.16	7.84	0.000121	***	0.475	0.000552	###
	Ndufs3	ENSMUSG00000005510	4.22	3.66	4.26	0.0349		0.953	0.154	
	Ndufs7	ENSMUSG00000020153	6.46	5.84	6.16	0.0153		0.916	0.285	
	Ndufs8	ENSMUSG00000059734	7.59	6.87	7.58	0.00022	***	0.953	0.007730	##
	Ndufv1	ENSMUSG00000037916	7.58	7.43	7.66	0.00287	**	0.748	0.633	
	Ndufv2	ENSMUSG00000024099	4.56	4.29	4.67	0.00744	**	0.808	0.588	
	Ndufa1	ENSMUSG00000016427	8.43	7.97	8.44	0.152		0.73	0.128	
	Ndufa10	ENSMUSG00000026260	1.59	1.55	1.55	0.000141	***	0.686	0.984	
	Ndufa11	ENSMUSG00000002379	6.82	6.15	6.74	0.14		0.986	0.002830	##
	Ndufa12	ENSMUSG00000020022	4.6	4.35	4.73	0.0636		0.683	0.269	
	Ndufa13	ENSMUSG00000036199	4.89	4.77	4.88	0.00851	**	0.987	0.736	
	Ndufa2	ENSMUSG00000014294	6.24	5.44	6.29	0.731		0.962	0.000477	##
	Ndufa3	ENSMUSG00000035674	7.71	7.20	7.75	0.627		0.982	0.0191	
	Ndufa4	ENSMUSG00000029632	6.23	5.71	6.41	0.151		0.982	0.0162	
	Ndufa4l2	ENSMUSG00000040280	7.32	6.79	7.41	0.836		0.922	0.0393	
	Ndufa5	ENSMUSG00000023089	7.96	7.39	8.09	0.00147	**	0.862	0.0053	##
	Ndufa6	ENSMUSG00000022450	7.27	6.79	7.42	0.419		0.912	0.0023	##
	Ndufa7	ENSMUSG00000041881	5.13	4.63	5.23	0.661		0.973	0.251	
	Ndufa8	ENSMUSG00000026895	4.26	3.52	4.16	0.000819	***	0.973	0.073	
	Ndufa9	ENSMUSG00000000399	8.68	7.99	8.42	0.029		0.965	0.092	
	Ndufab1	ENSMUSG00000030869	4.89	4.45	4.73	0.0645		0.796	0.470	
Complex-I	Ndufb10	ENSMUSG00000040048	6.39	6.02	6.60	0.0803		0.905	0.161	
	Ndufb11	ENSMUSG00000031059	8.41	7.68	8.50	0.0209		0.821	0.093	
	Ndufb2	ENSMUSG00000002416	7.46	6.71	7.31	0.0193		0.667	0.0028	##
	Ndufb3	ENSMUSG00000026032	5.92	5.38	6.31	0.272		0.988	0.043	
	Ndufb4	ENSMUSG00000022820	6.17	5.88	6.24	0.0485		0.946	0.378	
	Ndufb5	ENSMUSG00000027673	9.09	8.16	8.98	0.014		0.622	0.0000004	###
	Ndufb6	ENSMUSG00000071014	9.47	8.49	9.22	0.198		0.812	0.00133	##
	Ndufb7	ENSMUSG00000033938	6.82	6.41	6.86	0.338		0.856	0.021	
	Ndufb8	ENSMUSG00000025204	6.05	5.28	5.99	0.133		0.959	0.019	
	Ndufb9	ENSMUSG00000022354	1.15	1.15	1.78	0.000445	***	0.625	0.208	
	Ndufc1	ENSMUSG00000037152	5.45	4.88	5.49	0.235		0.673	0.309	
	Ndufc2	ENSMUSG00000030647	7.38	6.42	7.32	0.457		0.966	0.024	
	Ndufs4	ENSMUSG00000021764	6.88	6.31	6.90	0.0114		0.913	0.00010	###
	Ndufs5	ENSMUSG00000028648	8.15	7.47	8.02	0.896		0.573	0.011	
	Ndufs6	ENSMUSG00000021606	7.93	7.27	8.06	0.318		0.996	0.0016	##
	Ndufv3	ENSMUSG00000024038	5.51	4.87	5.66	0.0286		0.877	0.011	
	Sdha	ENSMUSG00000021577	10.2	9.34	10.10	0.00000896	***	0.75	0.000020	###
ComplexII	Sdhb	ENSMUSG00000009863	8.4	7.96	8.40	0.106		0.988	0.106	
	Sdhc	ENSMUSG00000058076	7.74	7.08	7.52	0.00496	**	0.557	0.047	
	Sdhd	ENSMUSG00000000171	8.27	7.79	8.15	0.0016	**	0.624	0.0102	
	mt-Cytb	ENSMUSG00000064370	12.9	12.10	12.80	0.00752	**	0.972	0.007	##
	Uqcr10	ENSMUSG00000059534	6.51	5.96	6.77	0.0852		0.72	0.016	
	Uqcr11	ENSMUSG00000020163	7.63	6.91	7.68	0.0126		0.961	0.008	##
ComplexIII	Uqcrb	ENSMUSG00000021520	6.55	6.30	6.74	0.461		0.821	0.202	
	Uqcrc2	ENSMUSG00000030884	9.51	8.88	9.37	0.00969	**	0.757	0.036	
	Uqcrfs1	ENSMUSG00000038462	8.15	7.56	8.18	0.0137		0.969	0.009	##
	Uqcrh	ENSMUSG00000063882	7.98	7.74	8.16	0.222		0.624	0.032	

	Uqcrq	ENSMUSG00000044894	6.11	5.53	6.23	0.181		0.952	0.126	
ComplexIV	mt-Co1	ENSMUSG00000064351	13.7	13.00	13.60	0.00297	**	0.811	0.007	##
	mt-Co2	ENSMUSG00000064354	6.87	5.68	5.62	0.0509		0.234	0.982	
	mt-Co3	ENSMUSG00000064358	5.72	5.46	5.15	0.73		0.669	0.681	
	Cox4i1	ENSMUSG00000031818	7.97	7.54	8.12	0.293		0.886	0.156	
	Cox4i2	ENSMUSG00000009876	0.968	1.01	0.58	0.999		0.756	0.519	
	Cox5a	ENSMUSG00000000088	7.88	7.07	7.79	0.000515	***	0.828	0.00111	##
	Cox5b	ENSMUSG00000061518	6.19	5.39	6.21	0.000978	***	0.975	0.00059	###
	Cox6a1	ENSMUSG00000041697	4.16	5.20	4.34	0.000147	***	0.683	0.00062	###
	Cox6a2	ENSMUSG00000030785	8.63	8.15	8.54	0.203		0.888	0.342	
	Cox6b1	ENSMUSG00000036751	7.44	7.07	7.66	0.593		0.889	0.376	
	Cox6c	ENSMUSG00000014313	7.63	7.28	7.59	0.145		0.933	0.208	
	Cox7a1	ENSMUSG00000074218	6.2	5.69	6.45	0.368		0.856	0.180	
	Cox7a2	ENSMUSG00000032330	5.66	5.33	5.75	0.296		0.961	0.229	
	Cox7a2l	ENSMUSG00000024248	6.95	6.85	7.18	0.675		0.548	0.121	
	Cox7b	ENSMUSG00000031231	5.73	5.52	5.95	0.544		0.772	0.205	
	Cox7c	ENSMUSG00000017778	6.78	6.56	7.00	0.483		0.621	0.094	
	Cox8a	ENSMUSG00000035885	2.51	3.46	2.83	0.0116		0.67	0.064	
	Cox8b	ENSMUSG00000025488	4.42	4.05	4.27	0.559		0.905	0.781	
ComplexV	mt-Atp6	ENSMUSG00000064357	5.98	4.64	4.98	0.24		0.595	0.876	
	Atp5a1	ENSMUSG00000025428	11	10.20	10.80	0.000163	***	0.578	0.00106	##
	Atp5b	ENSMUSG00000025393	11.6	11.10	11.50	0.00515	**	0.762	0.018	
	Atp5c1	ENSMUSG00000025781	10.1	9.50	10.00	0.00047	***	0.84	0.00090	###
	Atp5d	ENSMUSG00000003072	7.28	6.62	7.19	0.0484		0.869	0.099	
	Atp5e	ENSMUSG00000016252	7.12	6.83	7.21	0.24		0.897	0.131	
	Atp5f1	ENSMUSG00000000563	8.71	8.30	8.64	0.0385		0.869	0.078	
	Atp5g1	ENSMUSG00000006057	6.45	5.84	6.44	0.032		0.982	0.033	
	Atp5g2	ENSMUSG00000062683	5.49	4.87	5.30	0.0117		0.626	0.084	
	Atp5g3	ENSMUSG00000018770	9.36	8.98	9.41	0.0102		0.867	0.0032	##
	Atp5h	ENSMUSG00000034566	7.01	6.23	7.07	0.0045	**	0.966	0.0026	##
	Atp5j	ENSMUSG00000022890	7.75	7.08	7.73	0.032		0.969	0.036	
	Atp5j2	ENSMUSG00000038690	6.78	6.59	6.80	0.523		0.988	0.490	
	Atp5k	ENSMUSG00000050856	6.71	6.40	7.06	0.404		0.661	0.086	
	Atp5l	ENSMUSG00000038717	3.94	3.59	3.67	0.123		0.603	0.628	
	Atp5o	ENSMUSG00000022956	8.24	7.85	8.40	0.295		0.856	0.136	
	Atp5s	ENSMUSG00000054894	4.41	3.83	4.28	0.0129		0.811	0.043	

Full Uncut Western Blot Gel

Figure 1E- Western Blot Full Images

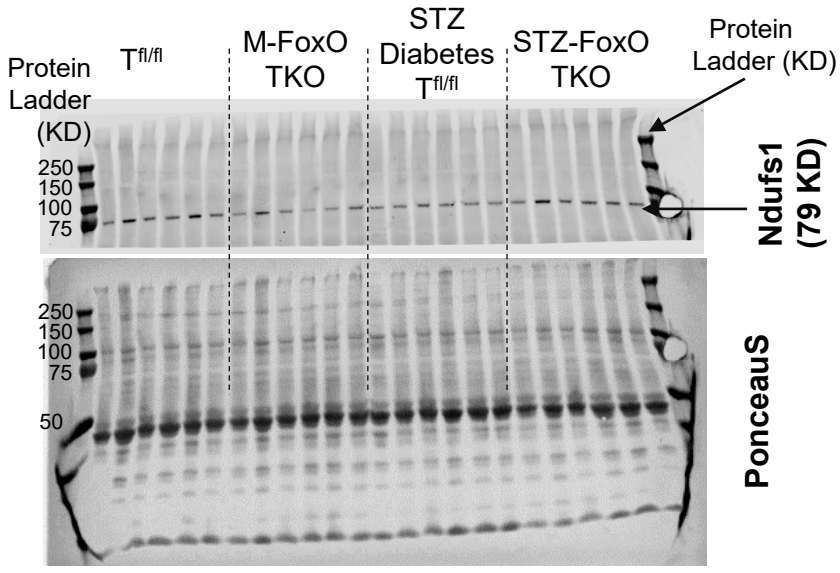

Figure 2A- Western Blot Full Images

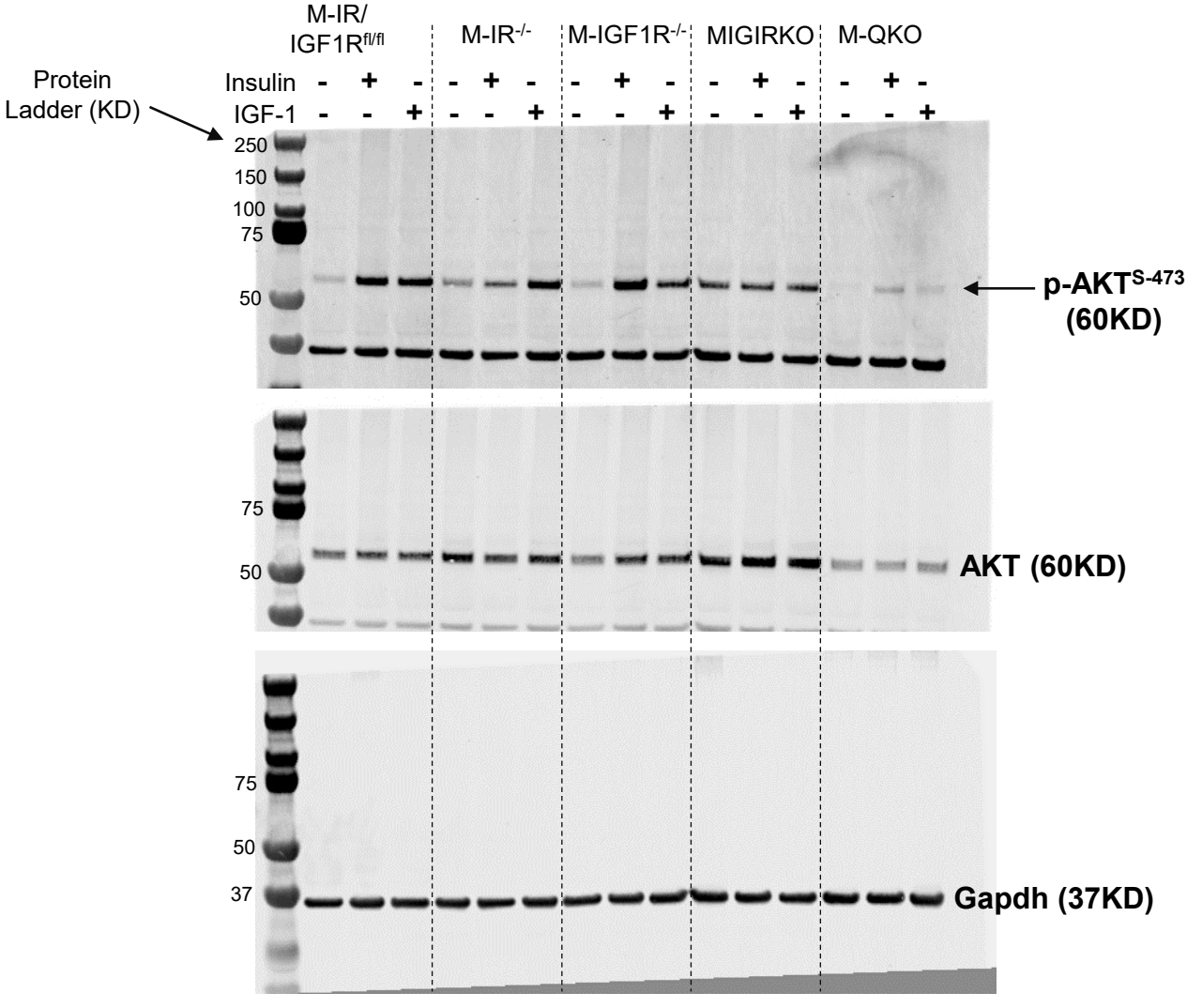

Figure 3K- Western Blot Full Images

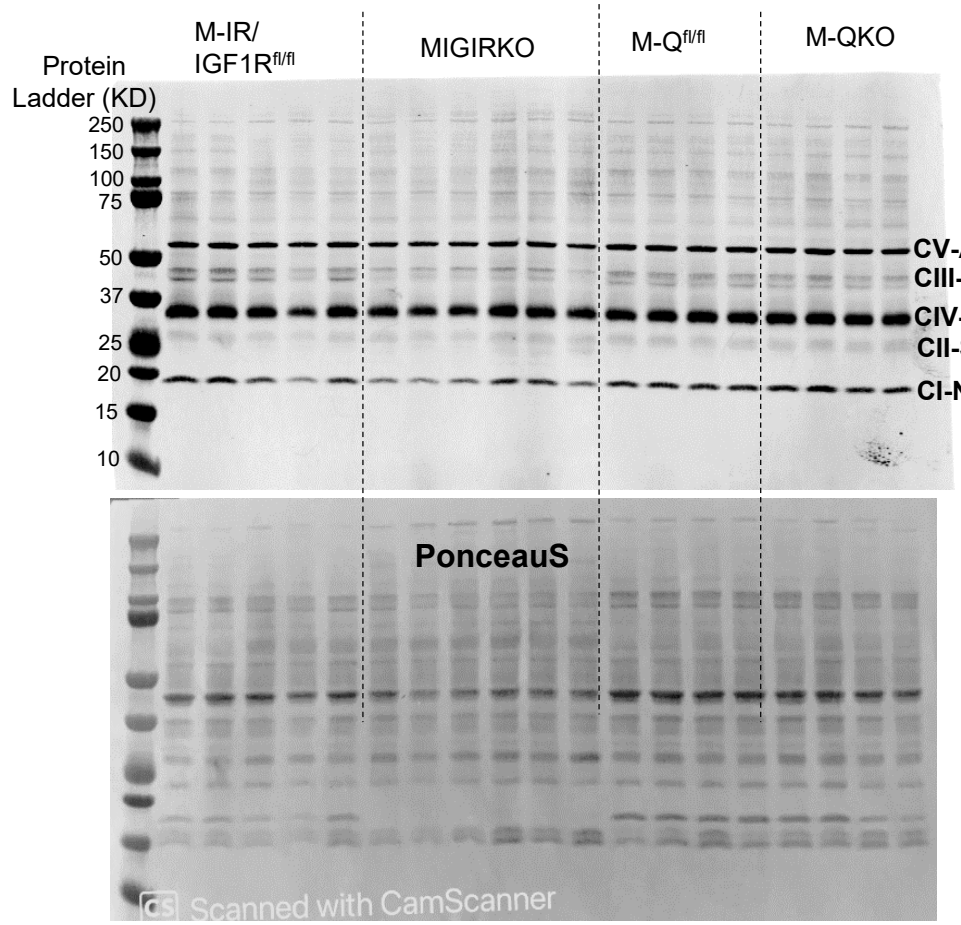

* This is a mtDNA encoded protein and migrate differently in different gel systems according to manufacturers (Ab 110413).

Figure 3N- Western Blot Full Images

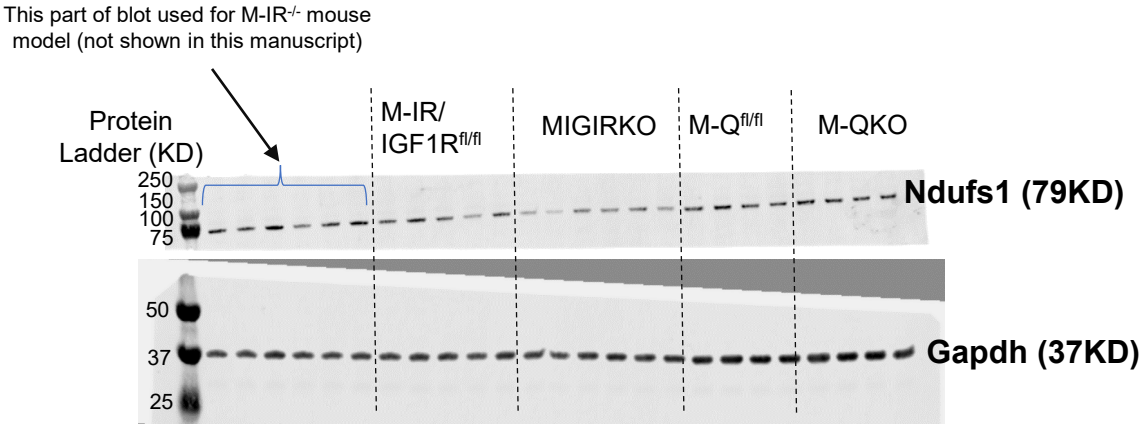

Figure 4M-Western Blot Full Images

Oxyblot showing carbonylation on proteins

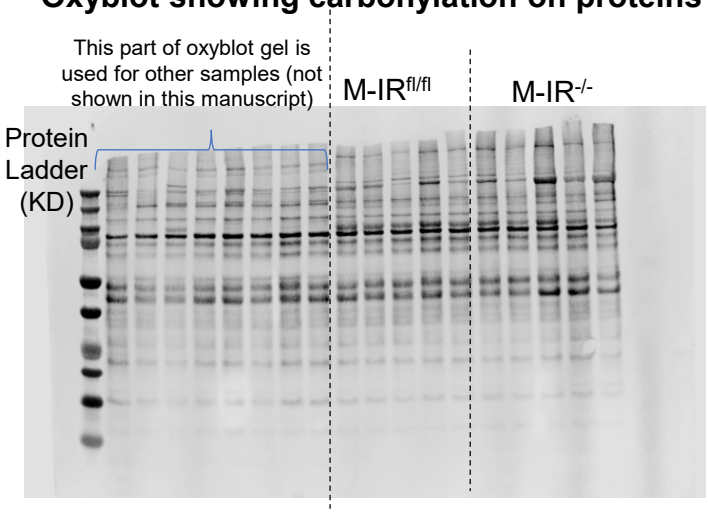

Ponceau S used for oxyblot

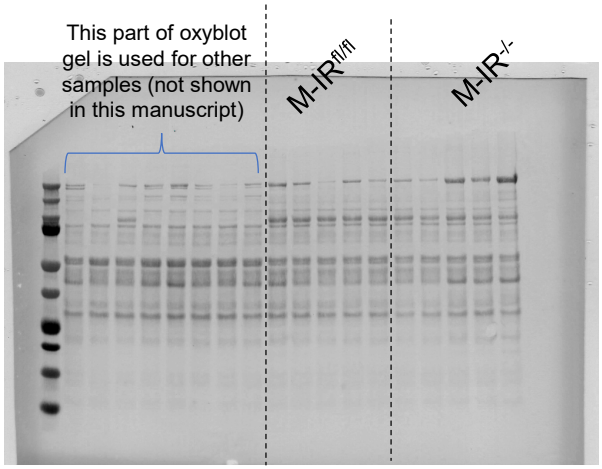

Figure 4N-Western Blot Full Images

Oxyblot showing carbonylation on proteins

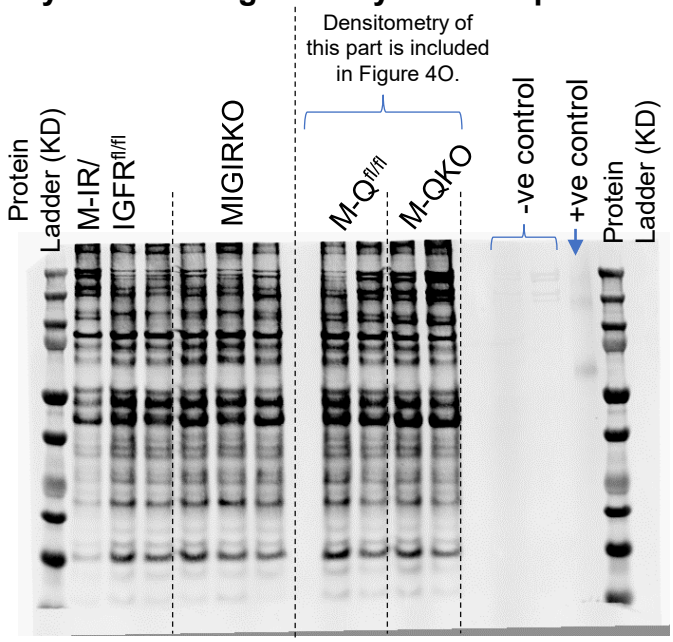

Vdac blot

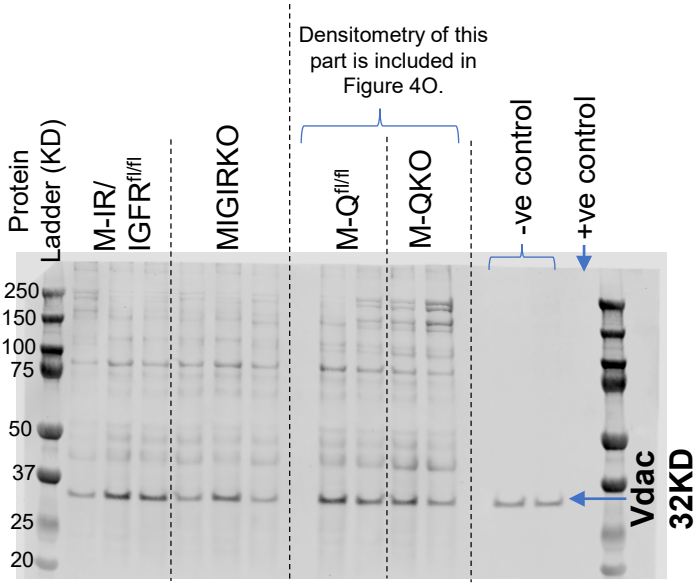

Figure 4O-Western Blot Full Images

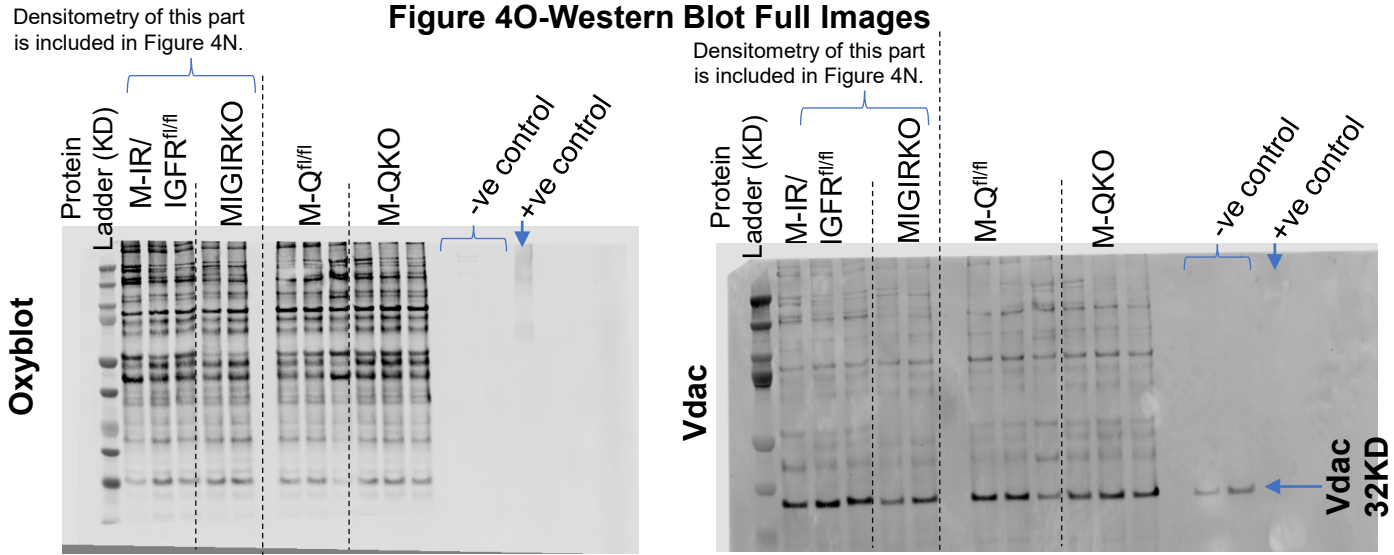

Figure 5B-Western Blot Full Images

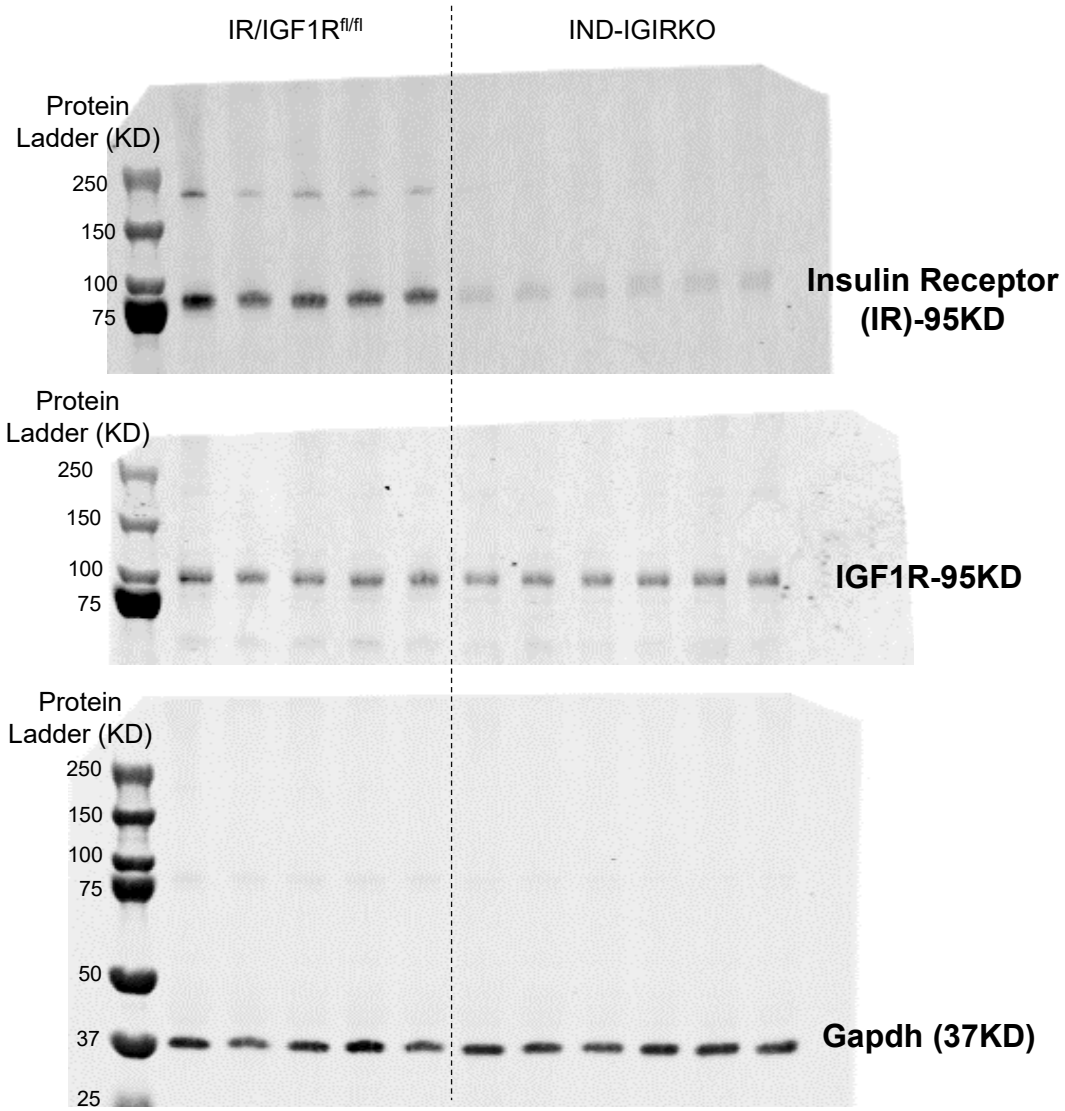

Figure 5M-Western Blot Full Images

OXPHOS

This blot is shown in main manuscript.

This blot is not shown in the main manuscript, but the densitometric quantification is added in OXPHOS densitometry (Figure 5N)

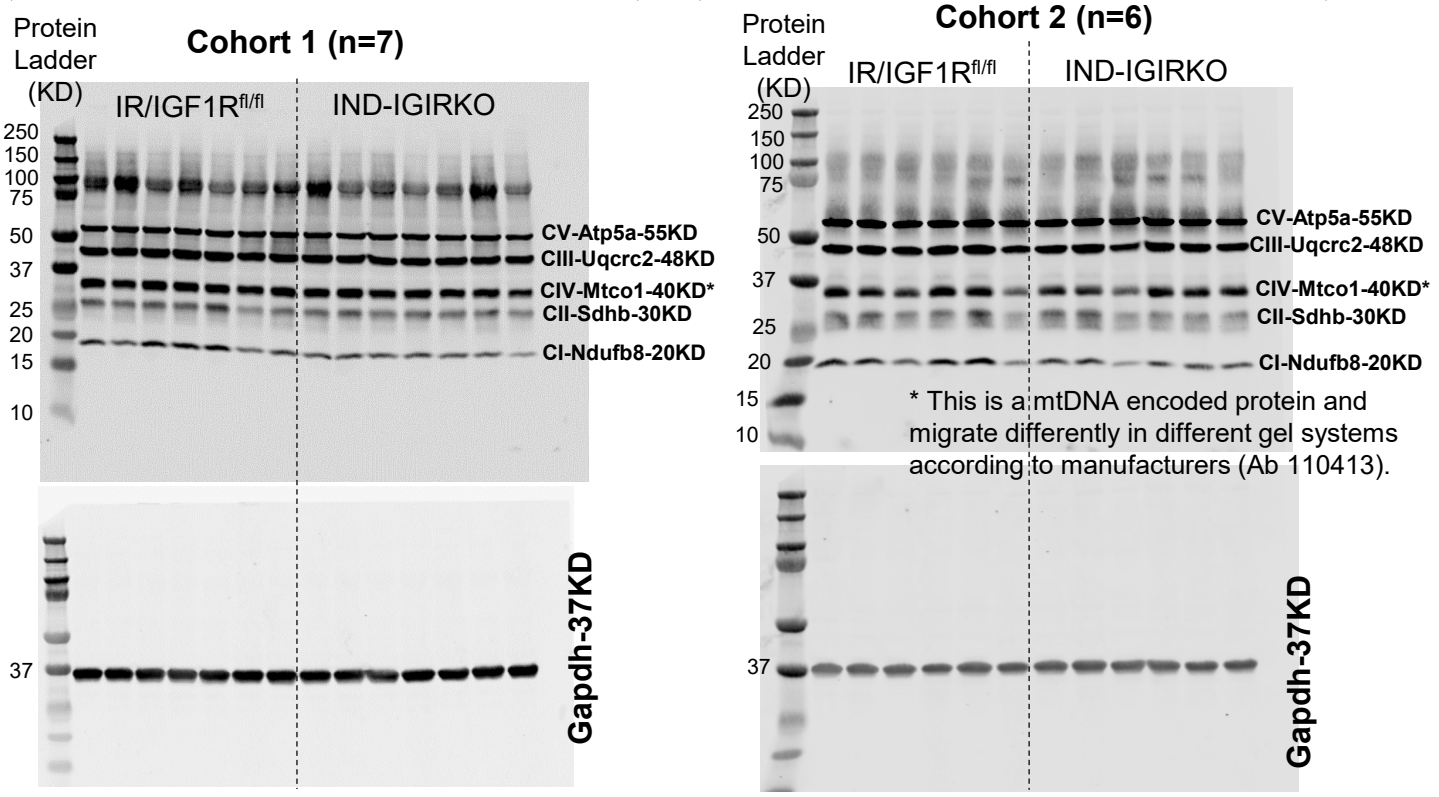

Figure 5M-Western Blot Full Images

Ndufs1

This blot is not shown in the main the manuscript, but the quantification from this is added in Figure 5O (Ndufs1 densitometry)

This blot is shown in main manuscript.

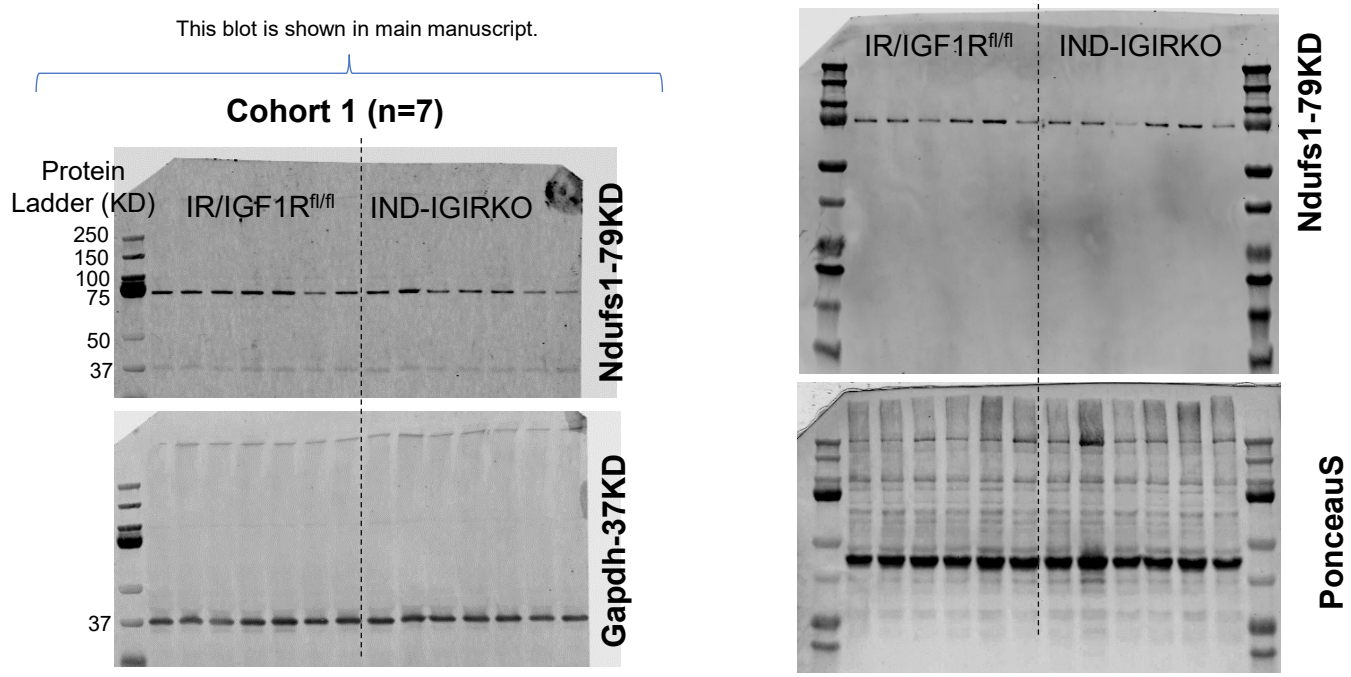

Figure 5M-Western Blot Full Images

Vdac

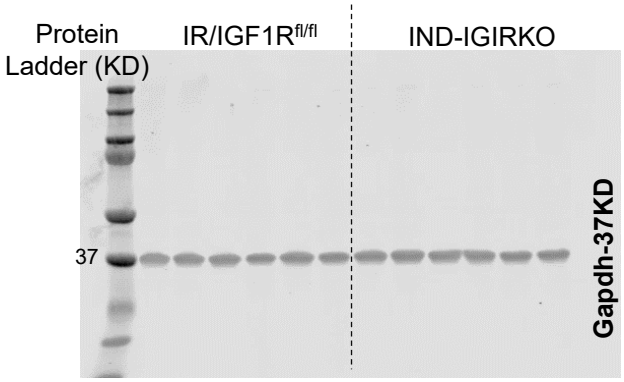

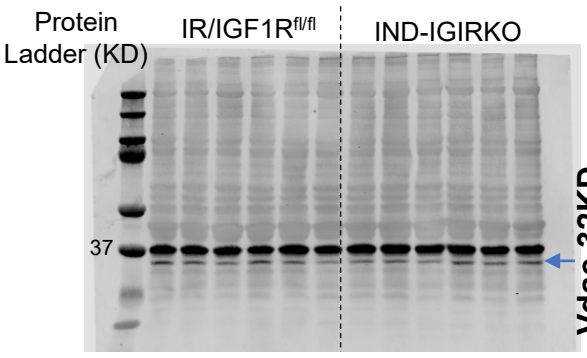

This is a stripped blot of Gapdh (shown in left side). Upper visible band in this blot is residual Gapdh after strip.

Figure 6A
Western Blot Full Images

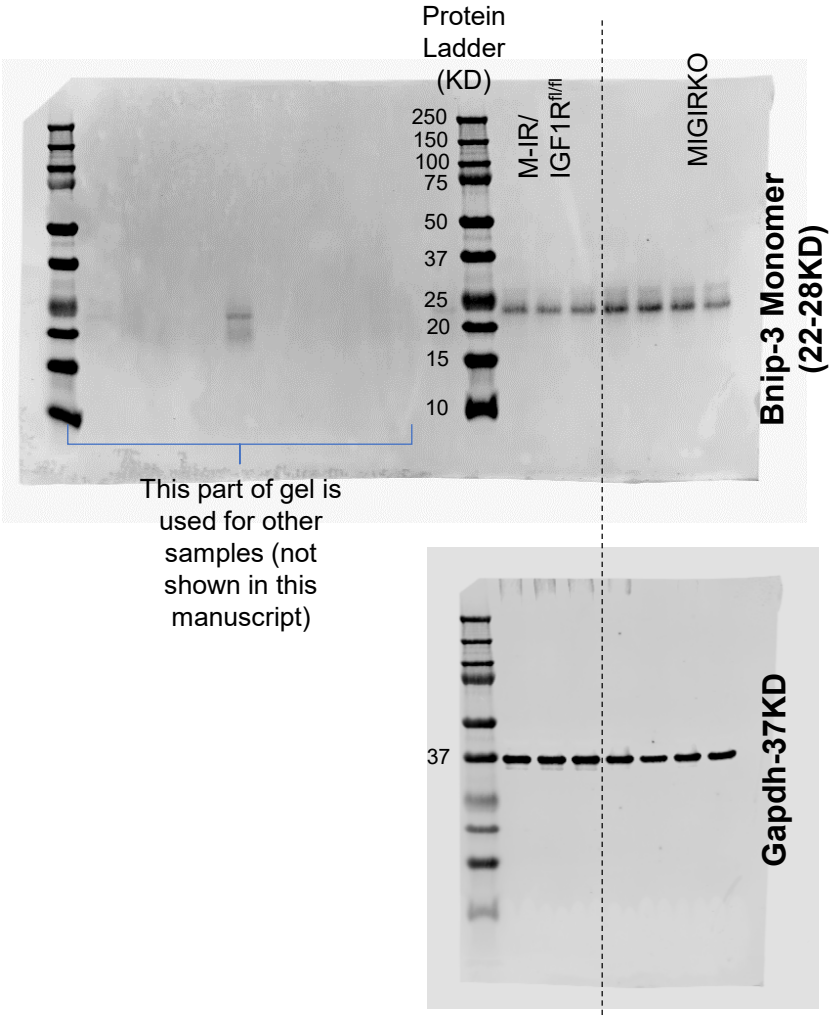

Figure 6B
Western Blot Full Images

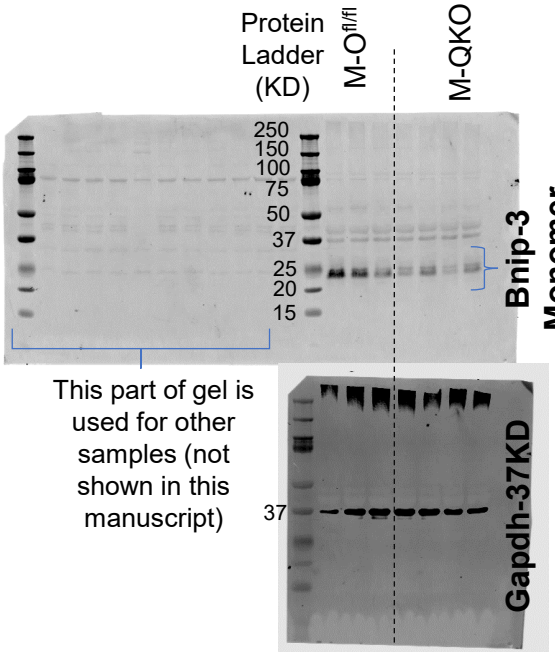

Figure 6C- Western Blot- Full Images

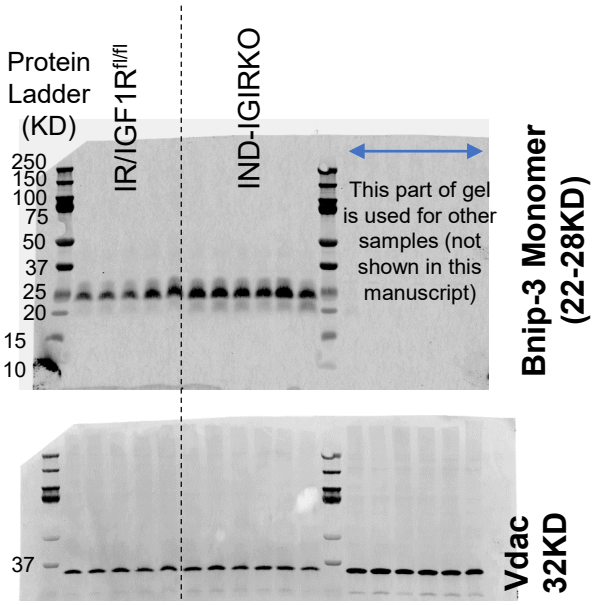

Figure 6E-Western Blot Full Images

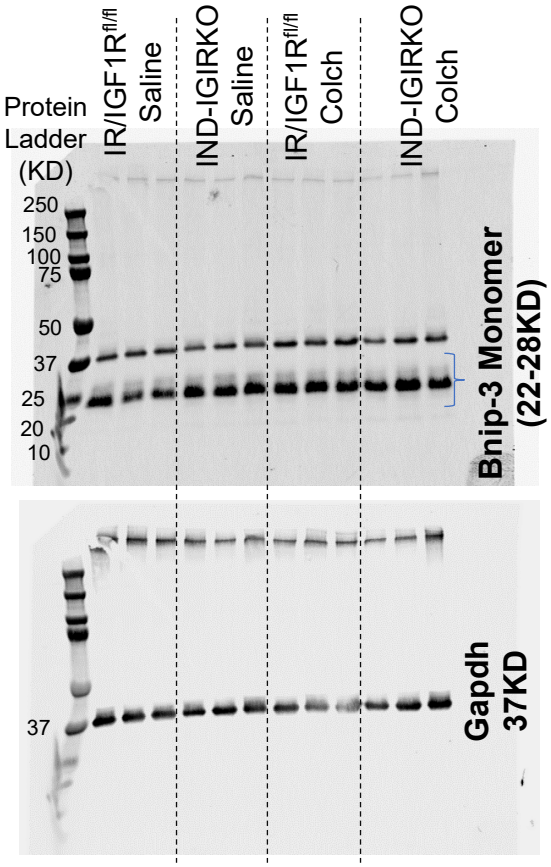

Figure 6G, and Supplemental Figure 6B- Western Blot Full Images

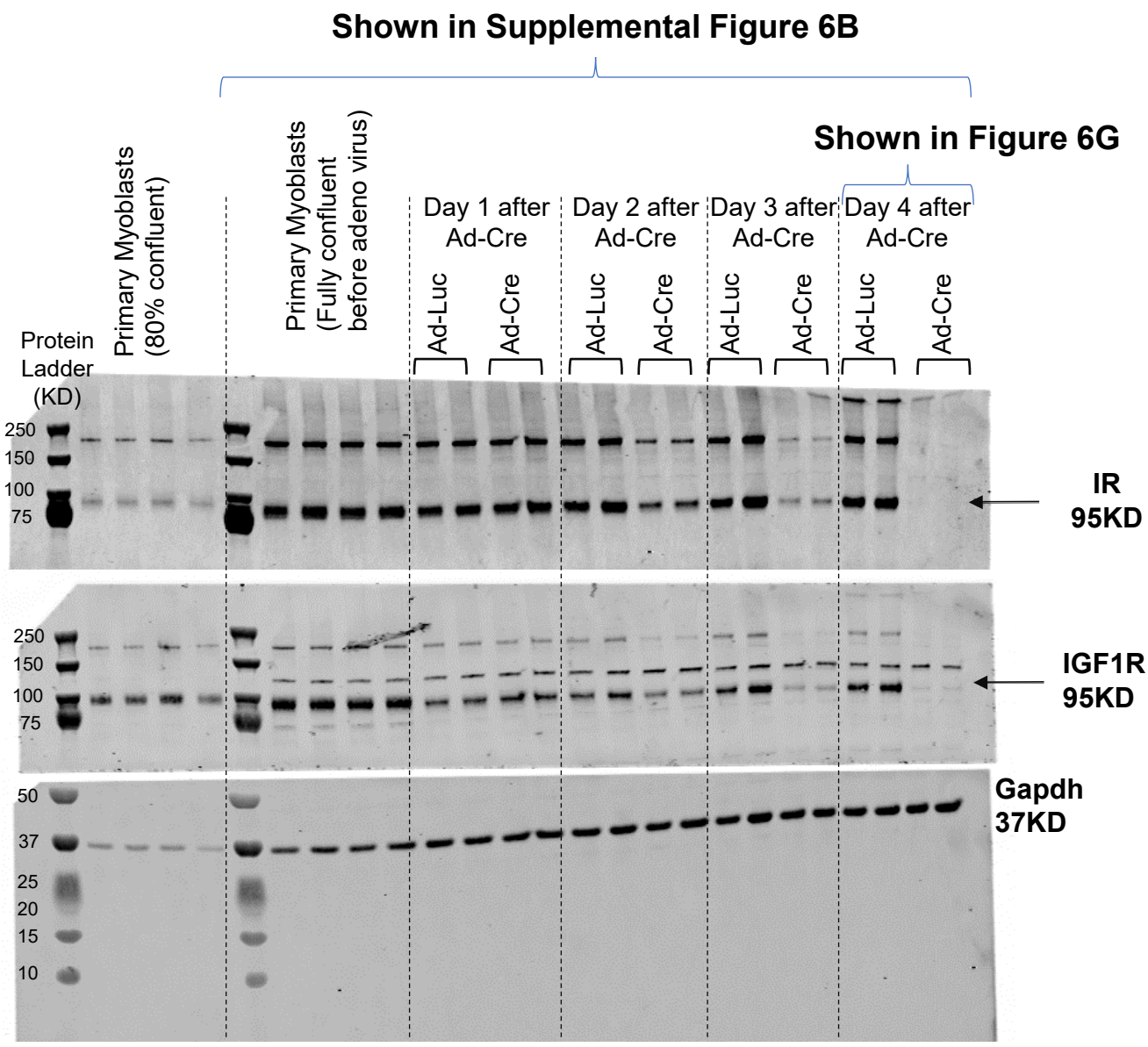

Supplemental Figure 1H- Western Blot Full Images

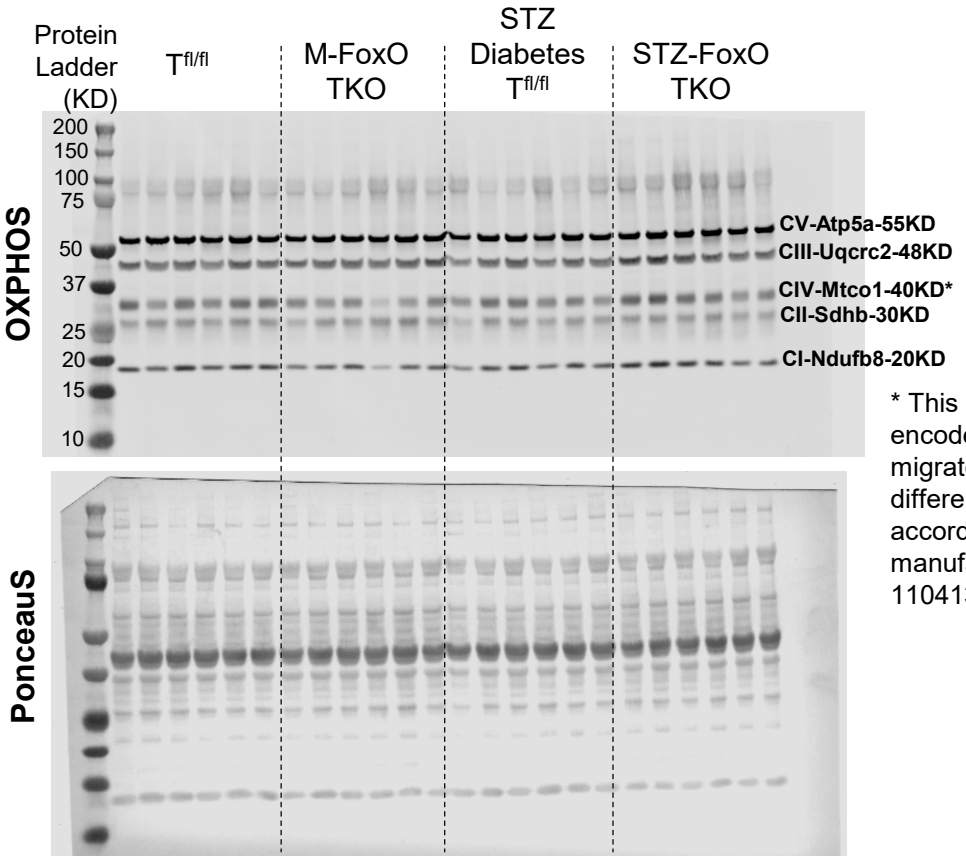

* This is a mtDNA encoded protein and migrate differently in different gel systems according to manufacturers (Ab 110413).

Supplemental Figure 2E-Western Blot Full Images

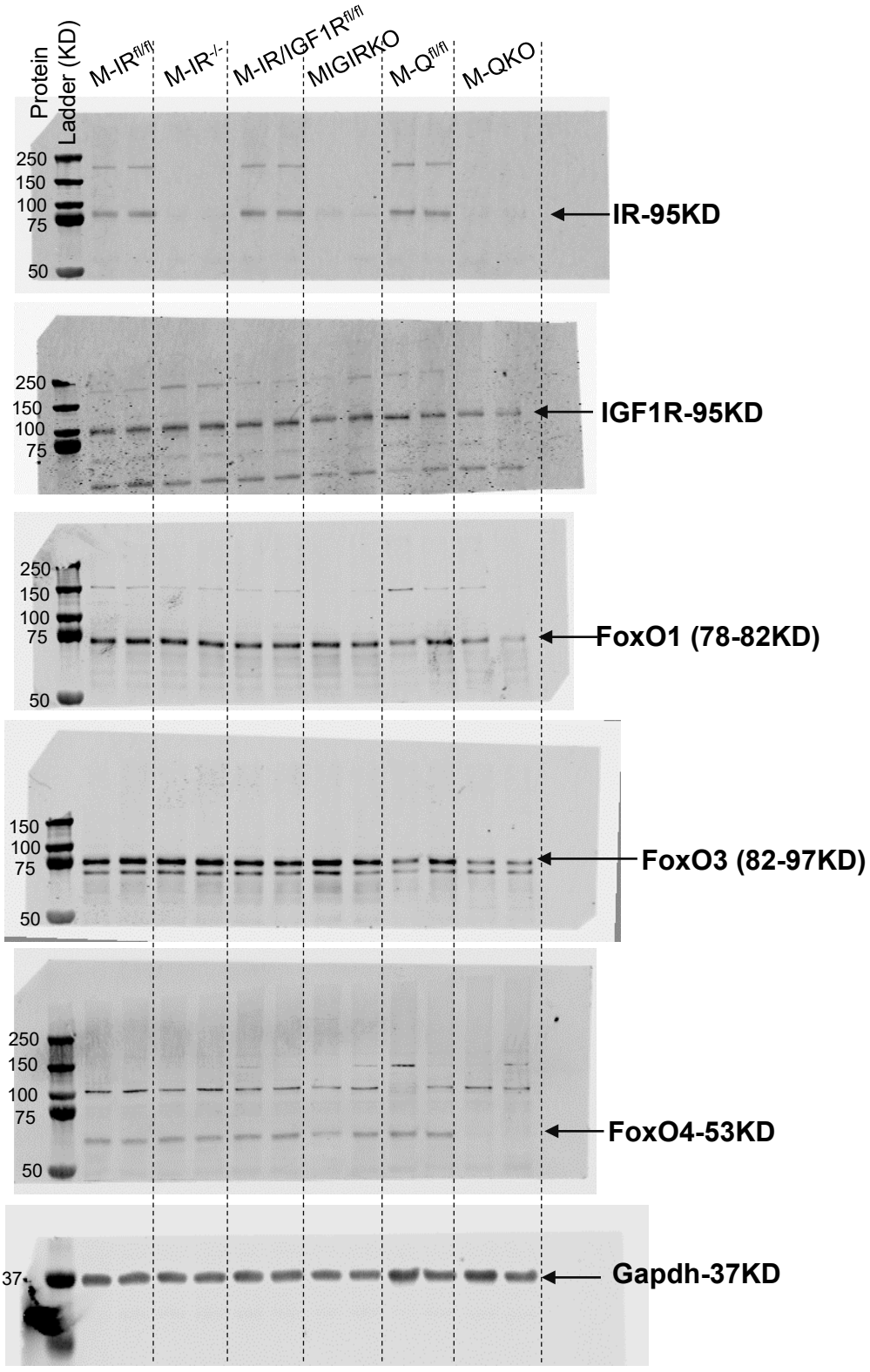

Supplemental Figure 2F-Western Blot Full Images

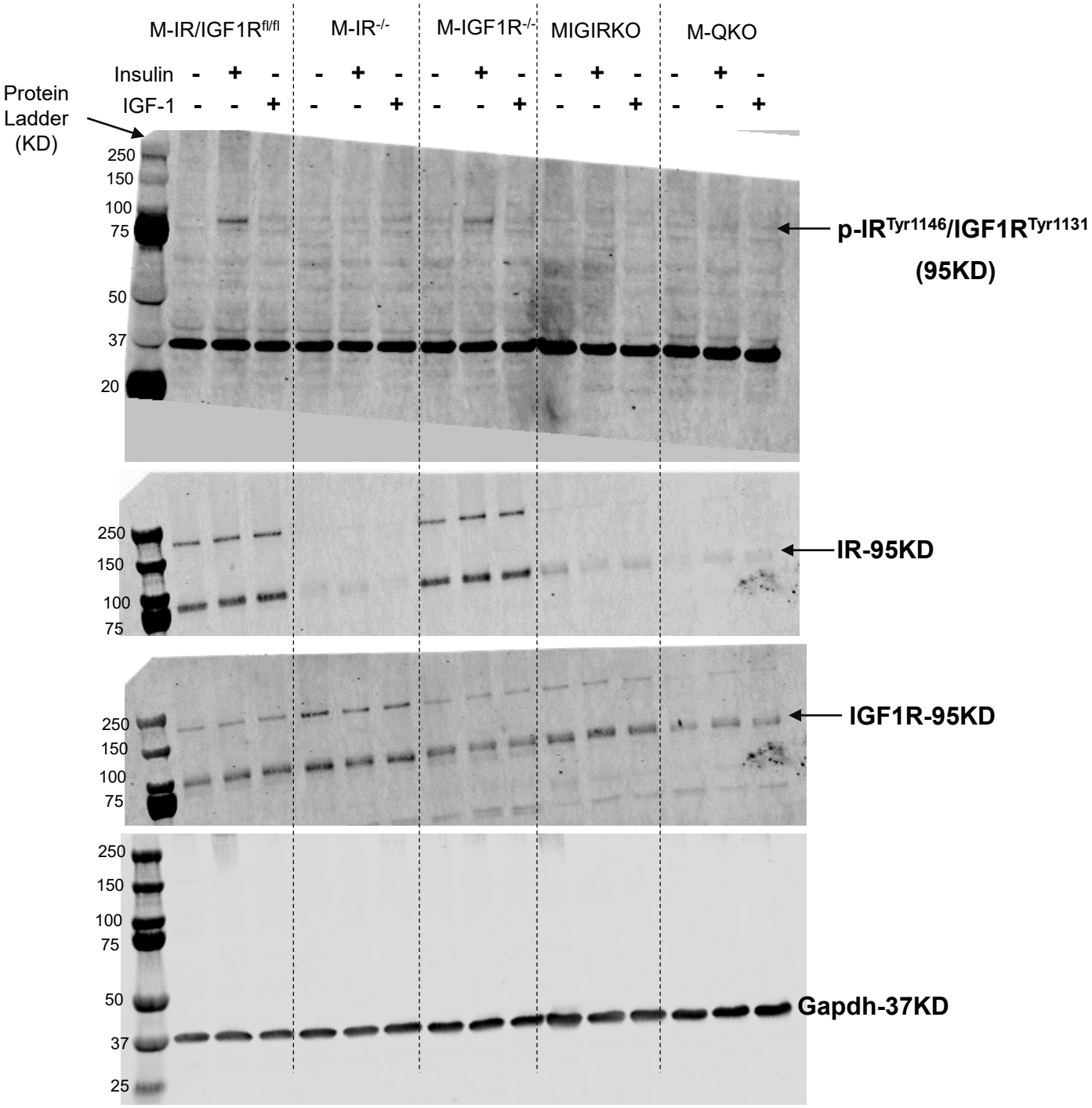

Supplemental Figure 2Q-Western Blot Full Images

Included in the densitometry (Supplemental figure 2R), but the image has not been shown in the main figure.

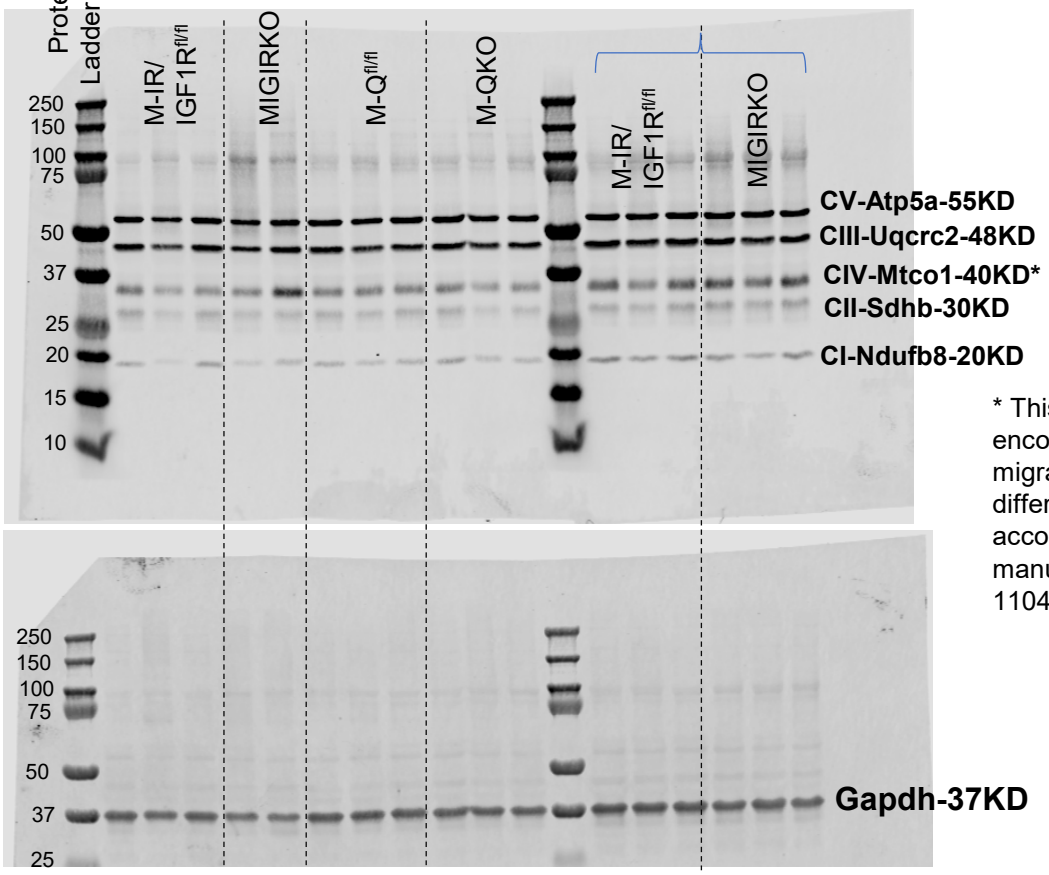

* This is a mtDNA encoded protein and migrate differently in different gel systems according to manufacturers (Ab 110413).

Supplemental Figure 2T-Western Blot Full Images

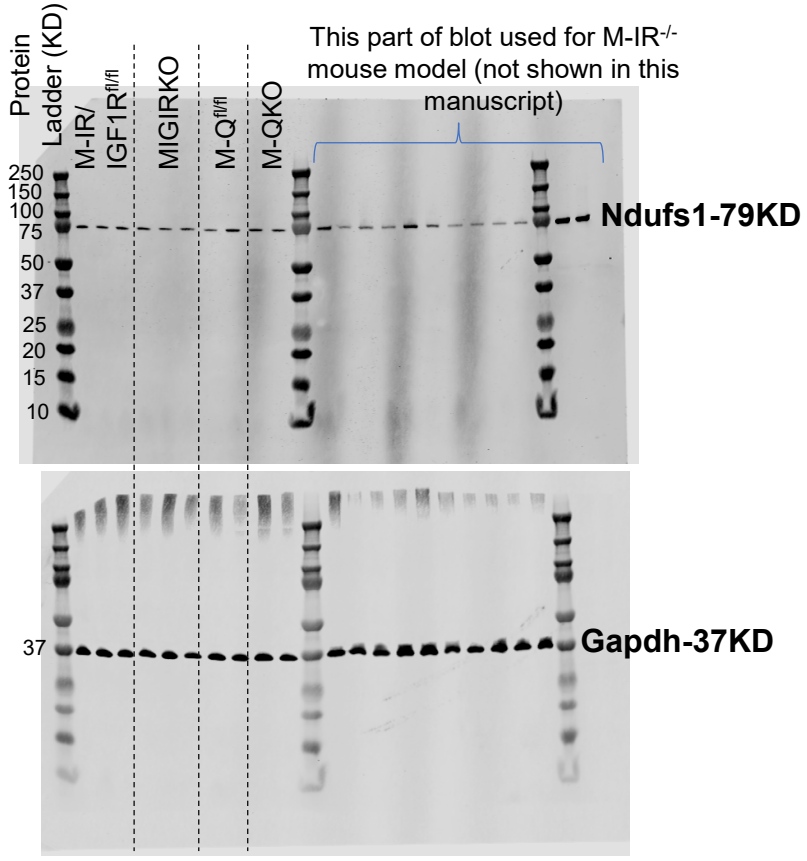

Supplemental Figure 3A (Western Blot Full Images)

Oxyblot showing carbonylation on proteins

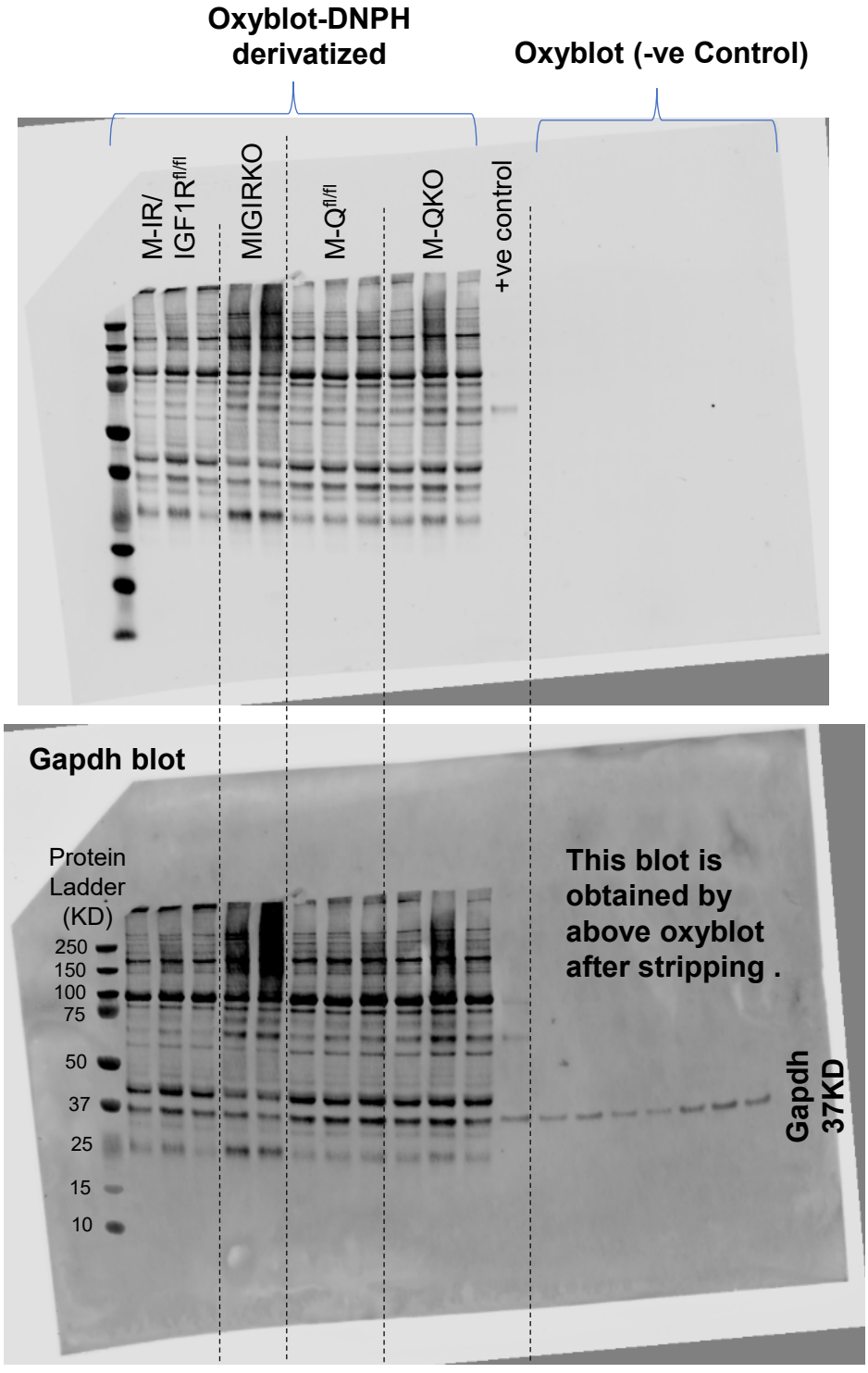

Supplemental Figure 3H
Western Blot Full Images

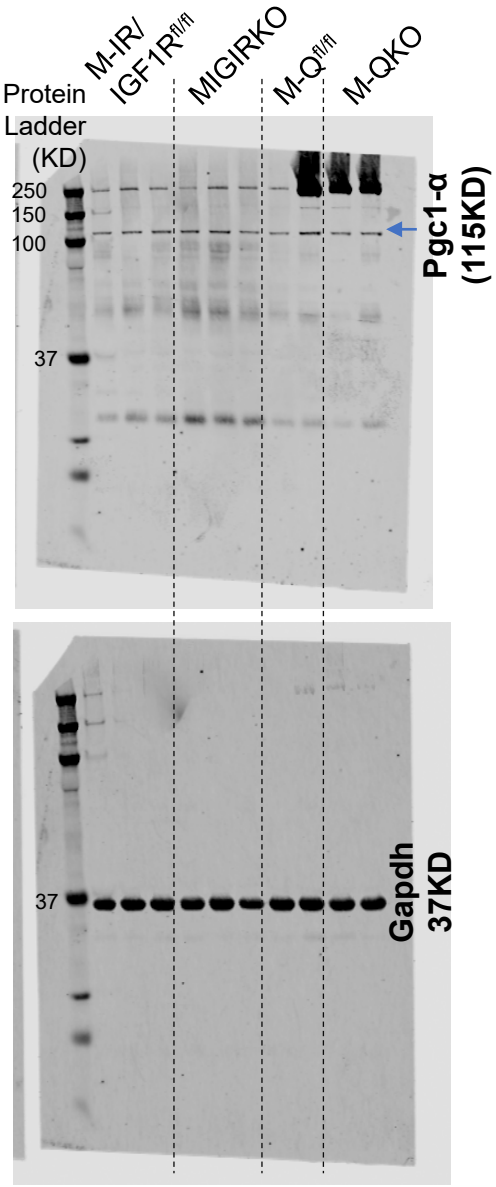

Supplemental Figure 3K
Western Blot Full Images

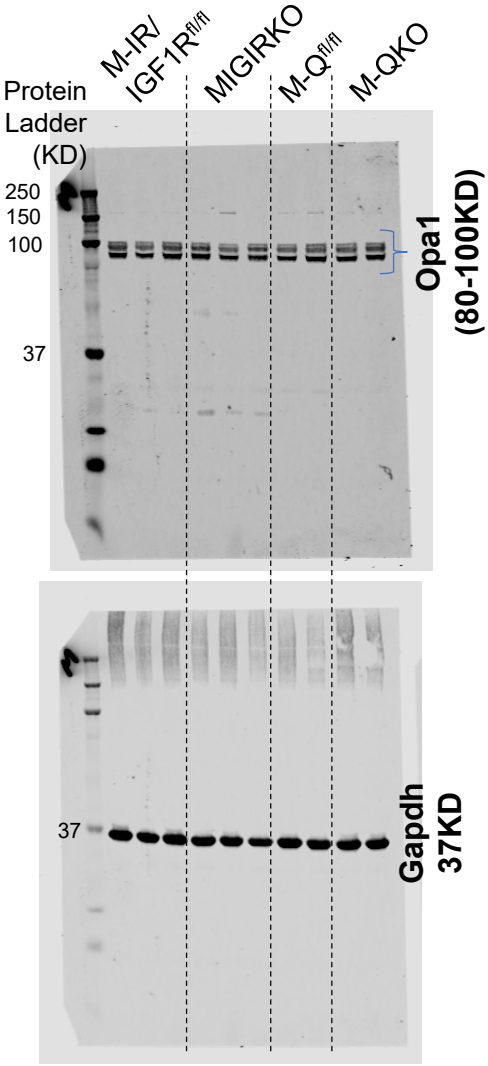

Supplemental Figure 3N- Western Blot Full Images

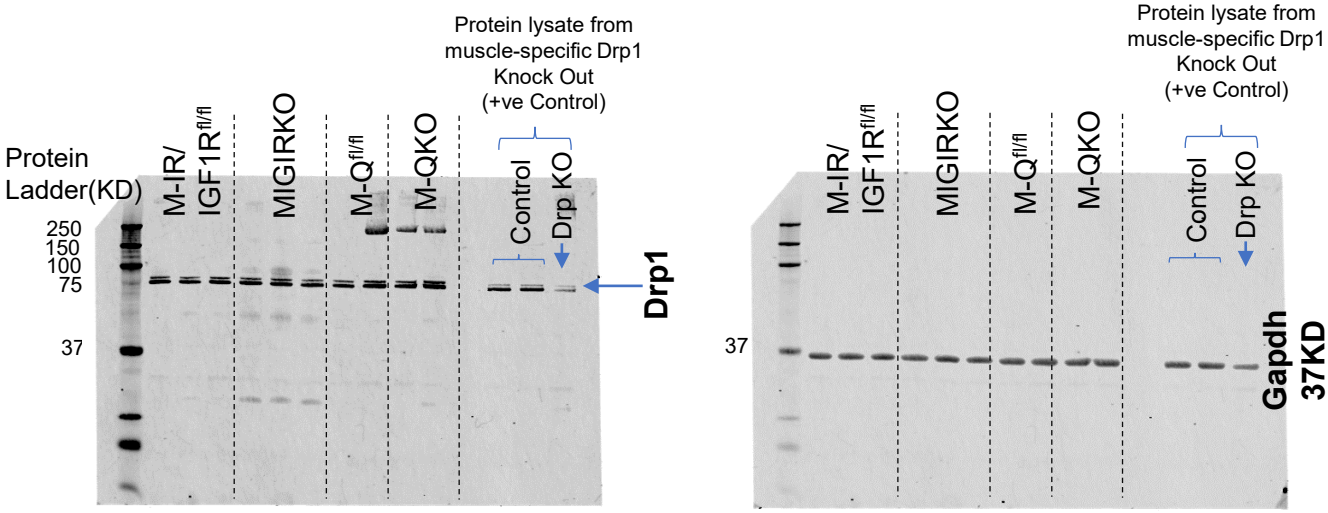

Supplemental Figure 4B-Western Blot Full Images

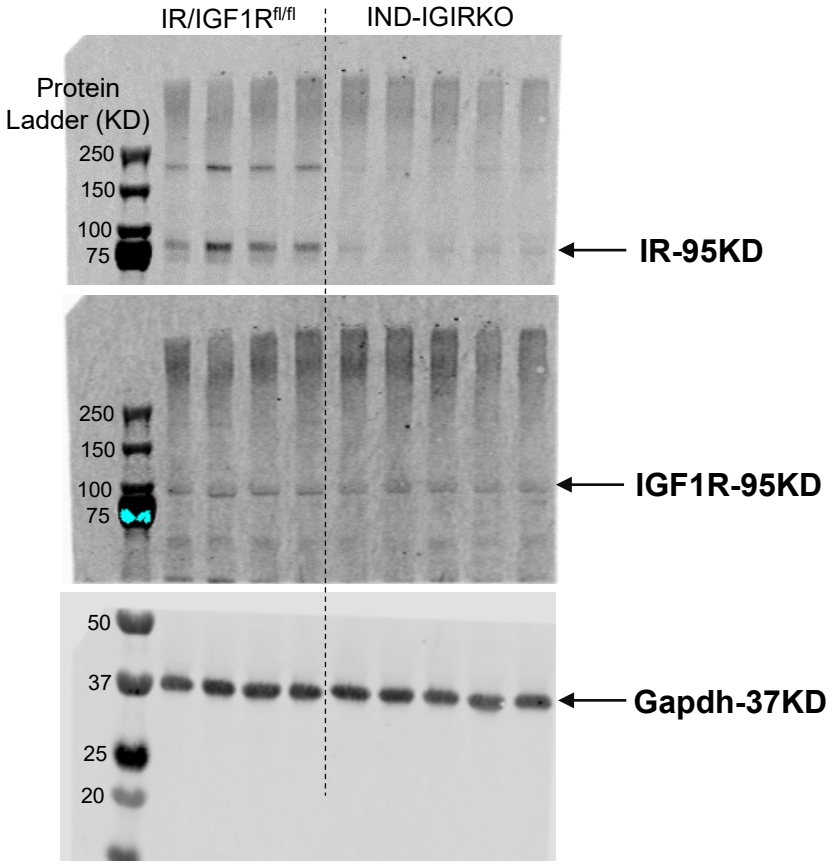

Supplemental Figure 4I Western Blot Full Images

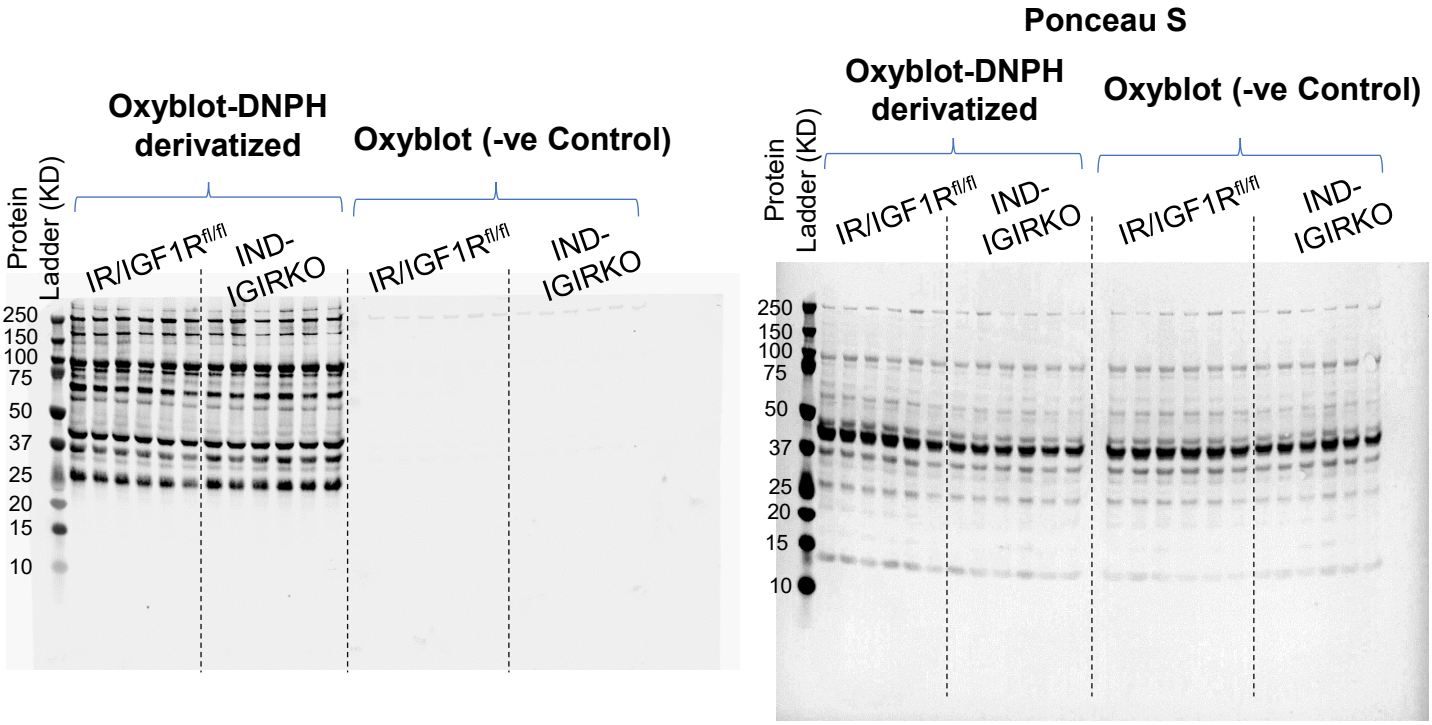

Supplemental Figure 4N, and 4O- Western Blot Full Images

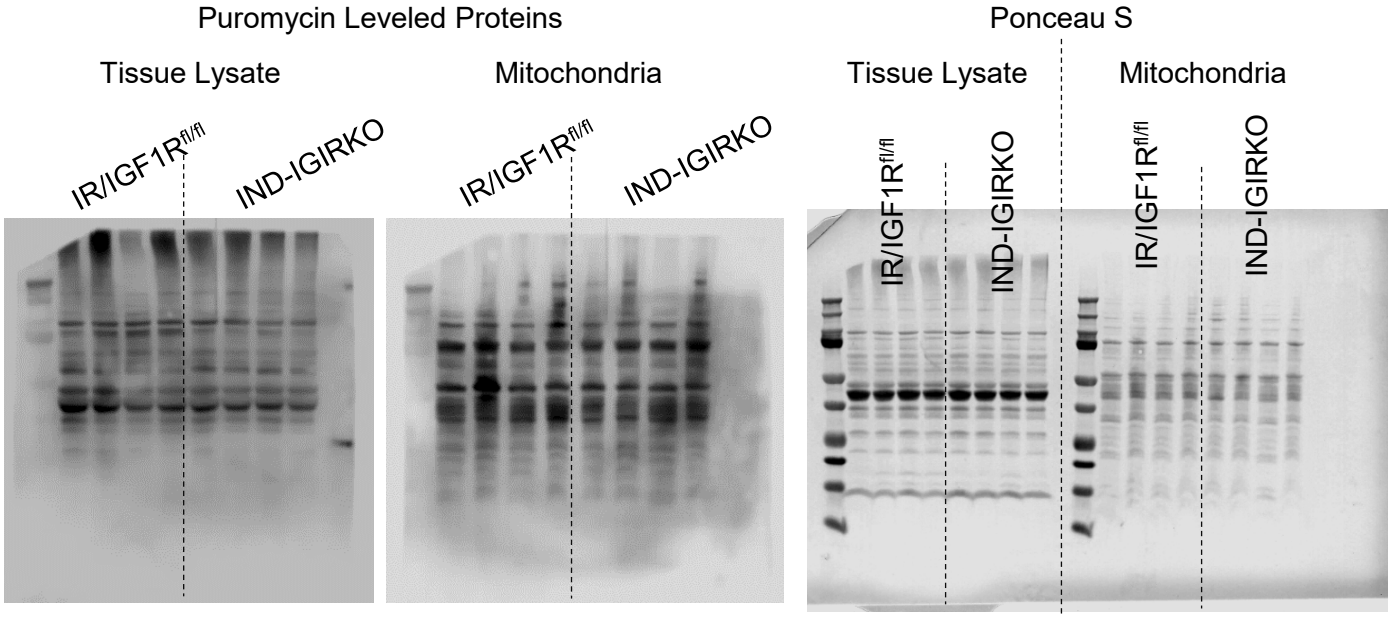

Supplemental Figure 4Q- Western Blot Full Images

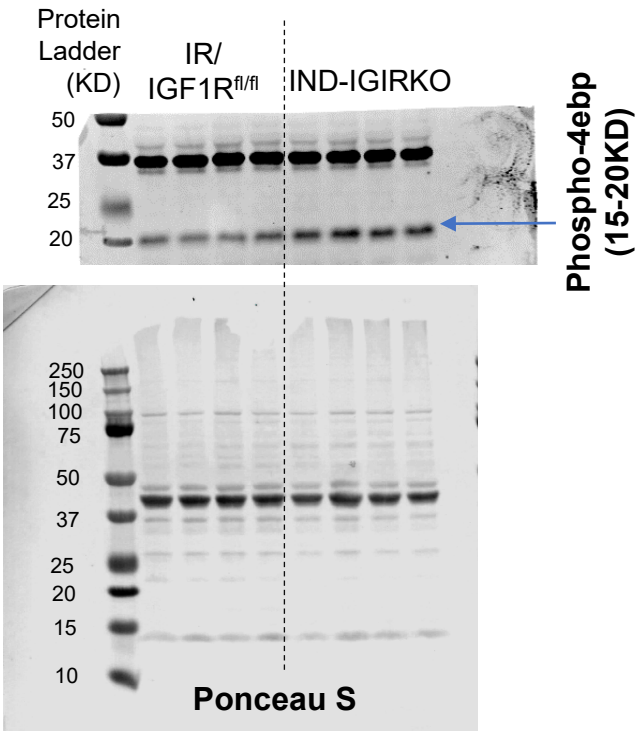

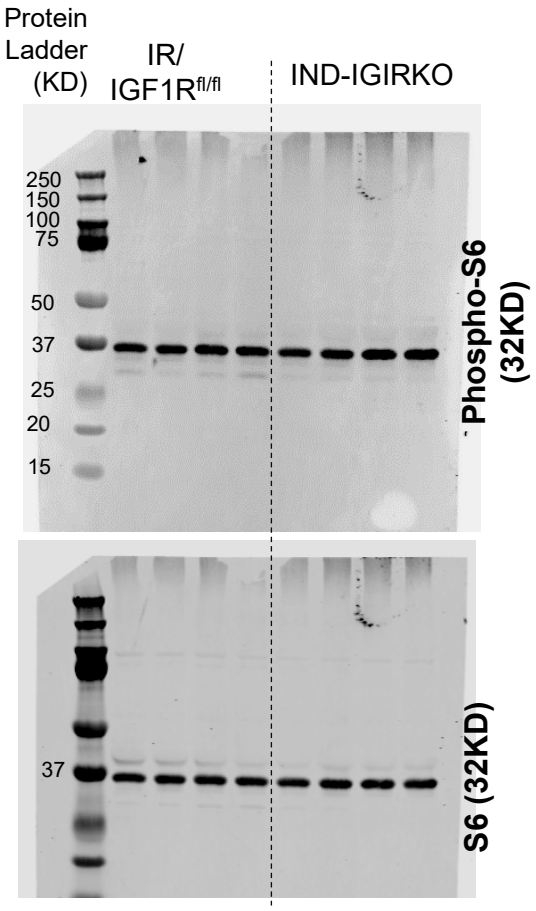

Supplemental Figure 4T Western Blot Full Images

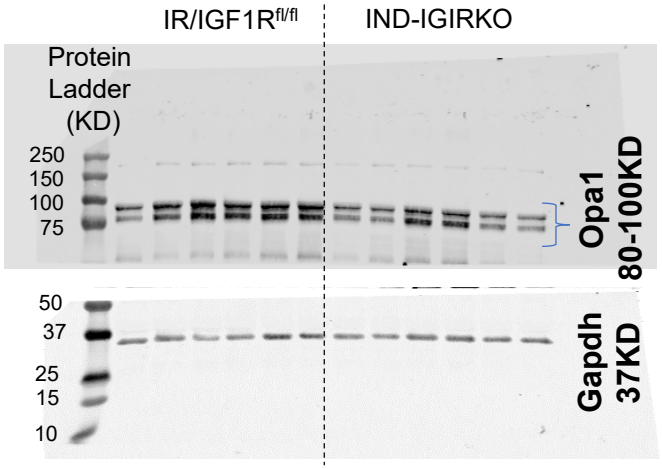

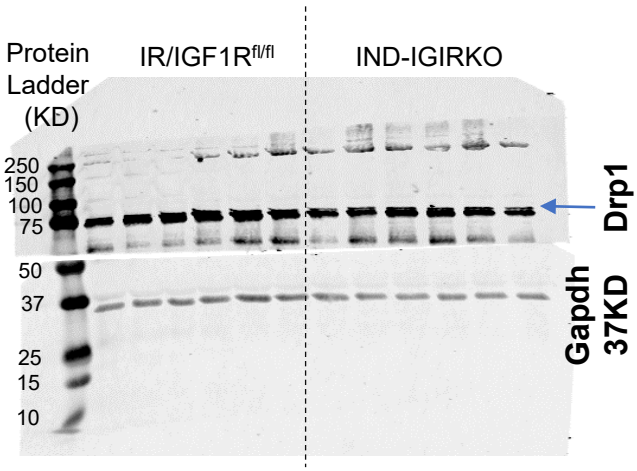

Supplemental Figure 5A Western Blot Full Images

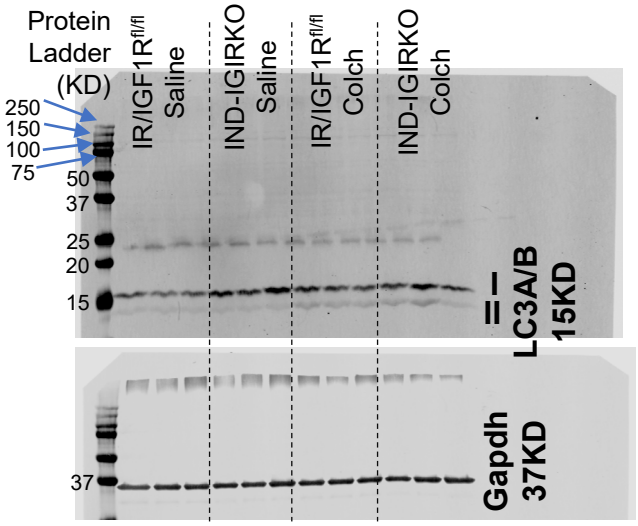

Supplemental Figure 5D Western Blot Full Images

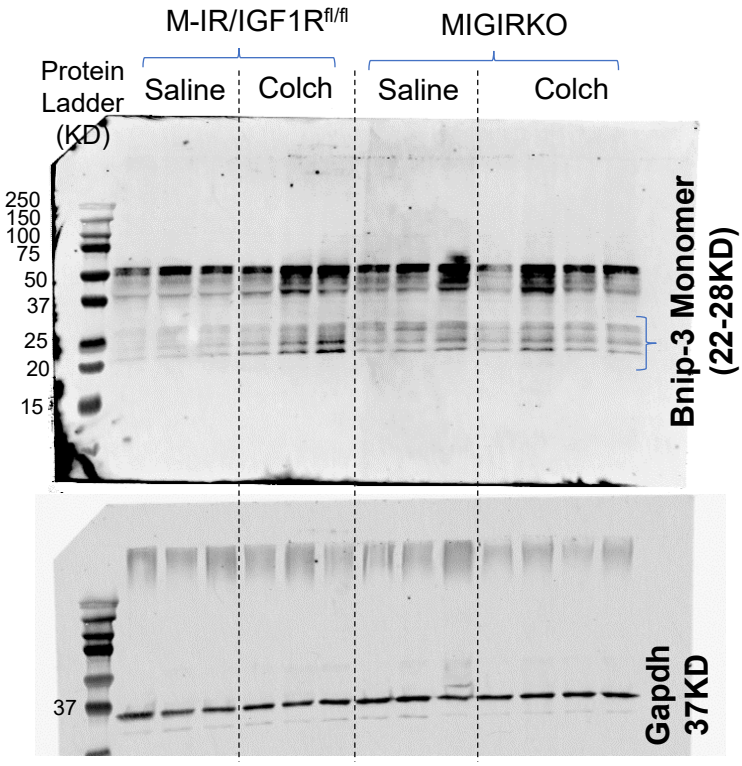

Supplemental Figure 5F- Western Blot Full Images

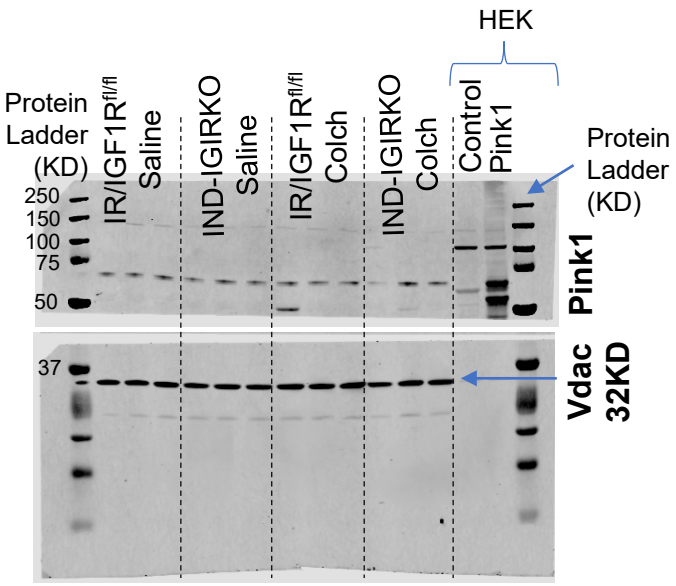

Supplemental Figure 6C- Western Blot Full Images